haematologica
Journal of the Ferrata Storti Foundation

Combining inotuzumab ozogamicin with the p38 inhibitor BIRB 796 and venetoclax exerts synergistic cytotoxicity in B-cell precursor acute lymphoblastic leukemia including very high risk t(17;19) acute lymphoblastic leukemia

by Lisa Fleischer, Hanna Kirchhoff, Caroline Schoenherr, Olaf Heidenreich, Michaela Scherr and Matthias Eder

Received: January 14, 2026.
Accepted: June 18, 2026.

Citation: Lisa Fleischer, Hanna Kirchhoff, Caroline Schoenherr, Olaf Heidenreich, Michaela Scherr and Matthias Eder. Combining inotuzumab ozogamicin with the p38 inhibitor BIRB 796 and venetoclax exerts synergistic cytotoxicity in B-cell precursor acute lymphoblastic leukemia including very high risk t(17;19) acute lymphoblastic leukemia.
Haematologica. 2026 June 25. doi: 10.3324/haematol.2026.300519 [Epub ahead of print]

Combining inotuzumab ozogamicin with the p38 inhibitor BIRB 796 and venetoclax exerts synergistic cytotoxicity in B-cell precursor acute lymphoblastic leukemia including very high risk t(17;19) acute lymphoblastic leukemia

Lisa Fleischer[1*], Hanna Kirchhoff[1*], Caroline Schoenherr[1], Olaf Heidenreich[2,3,4], Michaela Scherr[1#], Matthias Eder[1#]

*LF and HK contributed equally as co-first authors.
#MS and ME contributed equally as co-last authors.

[1]Hannover Medical School, Department of Hematology, Hemostasis, Oncology and Cell Therapy, Hannover, Germany
[2]Princess Maxima Center for Pediatric Oncology, Utrecht, The Netherlands
[3]University Medical Centrum Utrecht, Department of Hematology, Utrecht, The Netherlands
[4]Newcastle University, Wolfson Childhood Cancer Research Centre, Translational and Clinical Research Institute, Newcastle, United Kingdom

Running heads: p38 inhibition augments Inotuzumab efficacy in BCP-ALL

Corresponding author:
Matthias Eder
E-Mail: Eder.Matthias@mh-hannover.de

Data-sharing statement: Data supporting the findings of this study are available from the corresponding author upon reasonable request.

Acknowledgments: We thank Susanne Petri (Clinic for Neurology, Hannover Medical School, Germany) for providing us with mesenchymal stem cells. We acknowledge Iris Dallmann for excellent technical help and the staff of the Central Animal Facility of Hannover Medical School. This work was supported by Gerdes Stiftung Wolfsburg and H.W. & J. Hector-Stiftung.

Funding: This work was supported by Gerdes Stiftung Wolfsburg and H.W. & J. Hector-Stiftung.

Authors' disclosures and contributions: The authors declare no conflicts of interest.

Author contribution: LF is responsible for study concept, formal analysis, data curation, visualization, investigation, methodology, funding acquisition, and writing the original draft. HK is responsible for study concept, investigation, formal analysis, data curation, visualization, methodology, funding acquisition, and writing, reviewing and editing the manuscript. CS is responsible for investigation, writing, reviewing and editing the manuscript. OH is responsible for resources, reviewing and editing the manuscript. MS and ME are responsible for study design and supervision, project administration, funding acquisition, writing, reviewing and editing the manuscript.

Abstract

To improve mechanism-based pharmacotherapy for B-cell precursor acute lymphoblastic leukemia (BCP-ALL), we analyzed mode of action and potential synergies of inotuzumab ozogamicin (INO) with the p38 kinase inhibitor BIRB 796 and the BCL2-specific BH3 mimetic venetoclax (VEN) in BCP-ALL cell lines and patient-derived xenograft (PDX) models including t(17;19) PDX cells. INO is an antibody-drug conjugate (ADC) consisting of an anti-CD22 antibody linked to calicheamicin (CAL). CAL and INO induced DNA strand cleavage and activated DNA damage response signaling, including phosphorylation of ATM, H2AX (γH2AX) and p38, as well as induction of p53 protein expression. Pharmacologic inhibition of p38 with BIRB 796 selectively potentiated INO-induced DNA strand cleavage, increased γH2AX expression and enhanced cytotoxicity, whereas CAL activity remained unaffected in line with drug-interaction upstream of DNA damage. Furthermore, INO induced mitochondrial priming and augmented VEN-mediated mitochondrial outer membrane permeabilization, which was further enhanced by BIRB 796. Accordingly, INO and VEN exerted synergistic cytotoxicity in the presence and absence of BIRB 796. Finally, this triple therapy induced complete remissions assessed by bioluminescence imaging and long-term leukemia-free and overall survival in 5 out of 7 (71%) NSG mice engrafted with L707 (t(17;19)) PDX cells. These findings identify time-limited p38 inhibition as a mechanism-based strategy to enhance INO-induced DNA cleavage and mitochondrial priming, resulting in markedly improved therapeutic efficacy in a very high-risk leukemia model. This work may provide a rationale for optimizing ADC-based combination therapies through transient inhibition of p38.

Introduction

B-cell precursor acute lymphoblastic leukemia (BCP-ALL) is a heterogeneous malignancy with substantial variability in genetic, phenotypic, and clinical features. Despite advances in multi-agent pharmacotherapy, relapsed or refractory ALL (r/r ALL) remains associated with poor survival, with cellular therapies considered the only curative options. Some subtypes of very high-risk ALL, such as BCP-ALL with t(17;19)(q22;p13) encoding the fusion gene *TCF3::HLF*, are considered not curable with chemotherapy (1). Furthermore, high-risk ALL may relapse even after allogeneic stem cell transplantation, which by itself harbors significant morbidity and mortality, underscoring the need for novel pharmacotherapeutic strategies to prevent relapse, overcome resistance, and improve patient outcomes.

The antibody-drug conjugates (ADC) inotuzumab ozogamicin (INO) and gemtuzumab ozogamicin (GO) bind to the sialic-acid-binding immunoglobulin-like lectins CD22 (Siglec2) and CD33 (Siglec3) and are approved for r/r CD22-positive BCP-ALL and CD33-positive AML, respectively (2, 3). Both ADCs use identical linkers to couple calicheamicin γ1 (CAL), a highly potent enediyne antibiotic, to humanized monoclonal antibodies. Upon ADC binding and internalization, acid-labile lysosomal degradation releases CAL, which translocates to the nucleus and induces DNA strand breaks by phosphodiester cleavage, thereby activating DNA damage response (DDR) signaling (4-6). INO has shown synergistic activity with the BH3 mimetic venetoclax (VEN) in preclinical BCP-ALL models, providing a rationale for dual targeting of DDR pathways and mitochondrium-mediated apoptosis induction (7). VEN selectively binds to the BH3-binding groove of the anti-apoptotic protein BCL2, displacing sequestered pro-apoptotic proteins such as the activator BIM (8, 9). BIM activates oligomerization of the pro-apoptotic effector proteins BAK and BAX, inducing mitochondrial outer membrane permeabilization (MOMP), which is considered a point of no return for apoptosis induction (10). In our previous study, however, the combination of INO with VEN plus dexamethasone was insufficient to achieve long-term survival in the majority of mice engrafted with t(17;19) L707 patient-derived xenograft (PDX) cells despite drug synergy ex vivo (7). These findings underscore the need to further optimize INO- and VEN-based combination therapies in high-risk BCP-ALL.

The p38 mitogen-activated protein kinase (MAPK) pathway has emerged as a critical regulator of cellular stress responses, including those induced by DNA damage. Activation of p38 occurs through a kinase cascade leading to dual phosphorylation on conserved threonine/tyrosine (Thr/Tyr) residues within its activation loop (11). Four isoforms of p38 have been identified, with p38α being the best-characterized isoform primarily responsible for mediating stress-related signaling (12). The functional outcome of p38 activation is pleiotropic and highly context- and tumor type-dependent (11). In BCP-ALL, activation of p38 signaling has been associated with enhanced proliferation and cell survival (13). Interestingly,

pharmacological inhibition of p38 using small-molecule inhibitors such as BIRB 796 has already been shown to suppress leukemic cell growth as monotherapy in preclinical models in vivo (13).

We therefore analyzed the mode of action and potential synergies of INO, BIRB 796, and VEN both ex vivo and in vivo using BCP-ALL cell lines and PDX models including t(17;19) L707 cells. We show that the triple therapy acts highly synergistically and enhances remission rates, long-term leukemia-free and overall survival in 5 out of 7 L707 PDX engrafted NSG mice (71%).

Materials and Methods

Co-culture of PDX cells on human mesenchymal stem cells (MSCs)

MSCs isolated from healthy donors were kindly provided by Susanne Petri (14). Cells were seeded with $0.4x10^4$ MSCs per well of 96-well plates in MSC media (DMEM low glucose (Sigma-Aldrich, St. Louis, MO, USA), 20% FCS, 25 mM HEPES buffer (Gibco, Grand Island, NY, USA), 1% P/S, 2 ng/ml βFGF-2 (Gibco, Grand Island, NY, USA)) 24 h prior to adding PDX cells (15).

Comet Assay

Cells were analyzed by comet assay under alkaline and neutral conditions utilizing the Comet Assay Kit by Trevigen (Gaithersburg, MD, USA). Detailed experimental procedures are described in the Supplementary Material.

Generation of PDX cells and animal experiments

Primary patient samples were used in accordance with the Declaration of Helsinki after written informed consent of the respective patients and with approval from the ethical committee of Hannover Medical School for studies involving human blood or bone marrow (8345_BO_S_2019) for generation of PDX models in NSG mice. Further details are provided in the Supplementary Material.

For in vivo treatment experiments L707 PDX cells stably expressing luciferase ($1x10^6$) (15, 16) were intravenously transplanted into the tail veins of female NSG mice. Tumor burden was monitored by bioluminescence imaging (BLI) starting on day 13 post-transplantation. Mice were treated for three weeks and luminescence analysis was performed every 1-4 weeks to assess relapses and disease progression. Mice were euthanized upon reaching predefined clinical endpoint criteria. Animal experiments were approved by the Local Institutional Animal Care and Research Advisory Committee and permitted by the local authority (Lower Saxony State Office for Consumer Protection and Food Safety) (No. 33.14-42502-04 -19/3217 and No. 33.12-42502-04-21/3711).

Results

INO and CAL induce cytotoxicity and DNA strand cleavage

We first evaluated the cytotoxic effects of either the intact ADC INO or its cytotoxic payload CAL in BCP-ALL cell lines. For 697 and NALM-6 cells, the IC50 for INO (660 pM and 6600 pM) were 88- and 330-fold higher than for CAL (7.5 pM and 20 pM) (Supplementary Figure S1A-D), in line with only a small portion of CAL conjugated to INO released intracellularly. We next investigated INO- and CAL-induced DNA strand cleavage at their respective IC50s using the comet assay under alkaline conditions. As CAL exerts its cytotoxic activity almost immediately upon incubation, whereas INO displays a delayed response due to internalization and ADC cleavage (17), comet assays were performed after 2 h for CAL and 6 h for INO treatment. Although both CAL and INO induced DNA strand cleavage, INO-induced DNA cleavage was weak, whereas CAL induced high levels of strand breaks under these conditions (Figure 1A).

We then analyzed the dependence of CAL-induced DNA strand cleavage on time, dose, and temperature. The amount of in tail DNA increased in a dose- and time-dependent manner upon CAL treatment in 697 cells (Figure 1B-D). Furthermore, CAL-induced DNA strand cleavage was temperature-dependent, with 697 cells incubated with CAL on ice showing no detectable DNA strand breaks. In contrast, incubation at 37°C induced strong DNA fragmentation (Figure 1E). We next analyzed CAL-induced double strand breaks (DSBs) using the comet assay under neutral conditions (without alkaline-induced DNA denaturation), thereby mainly detecting DSBs. DSBs are quantified by the tail moment, the product of tail length and the percentage of DNA in the tail (18). At concentrations that induced approximately 90% in tail DNA in alkaline comet assays for all treatment conditions (Figure 1F), CAL caused significantly more DSB (tail moment of about 20) than other DDR inducers such as the topoisomerase-II inhibitor etoposide (ETO) or γ-irradiation (Figure 1G). Almost identical results were observed in NALM-6 cells (Supplementary Figure S1E-J).

CAL and INO induce DDR signaling and phosphorylation of p38

To investigate induction of DDR signaling, 697 and NALM-6 cells were treated with CAL or INO at their IC50 (Figure 2 and Supplementary Figure S2A). CAL induced phosphorylation of ATM at Ser1981 and of histone H2AX at Ser139 (γH2AX) in a time-dependent manner. In addition, phosphorylation of p38, p53 protein expression, and cleavage of PARP1 were induced, indicating that DDR signaling triggers initiation of apoptosis. In contrast, p38α protein expression levels were largely unaffected.

Induction of DDR signaling seemed dependent on ATM as an initial event, since pharmacological ATM inhibition with KU-60019 reduced the downstream signaling events

described above. KU-60019 blocked ATM auto-phosphorylation and reduced cell growth by 60-70% (Supplementary Figure S2B-C). Besides pharmacological inhibition of ATM function, stable reduction of ATM protein expression using lentiviral-encoded shRNAs (SEW-ATMsh) produced similar results. Reducing ATM expression severely impaired cell growth by 75% compared to control cells and reduced INO-induced γH2AX, p53, pp38, and cleaved PARP1 signals (Supplementary Figure S2D-F).

Interestingly, INO induced DDR signaling comparable to CAL at the respective IC50, but in a delayed manner, consistent with the time required for intracellular CAL release from INO (17).

Pharmacological inhibition of p38 with BIRB 796 enhances INO-mediated DNA strand cleavage and augments DDR signaling and cytotoxicity

BIRB 796 is a pharmacological p38 inhibitor that inhibits p38 auto-phosphorylation. In 697 and NALM-6 cells, phosphorylation of p38 (pp38) was reduced by 60-70% after 4 h of BIRB 796 treatment and persisted after 24 h and 48 h of treatment (Supplementary Figure S3A-C). In addition, treatment with BIRB 796 resulted in a dose-dependent reduction in cell growth compared to control cells (Supplementary Figure S3D+E). 1 µM BIRB 796 reduced cell growth by approximately 60% compared to the control, whereas 10 µM BIRB 796 further decreased cell growth by 80-90%. Treatment of 697 and NALM-6 cells with 1 µM BIRB 796 did neither affect cell viability nor induce signals of DNA fragmentation in comet assays under alkaline conditions after 24 h or 48 h. BIRB 796 affected cell viability only at ultra-high concentrations (10-50 µM) after 48 h of treatment, with cell viability of about 75% (Supplementary Figure S3F-I).

Interestingly, BIRB 796 potentiated INO-induced cytotoxicity (Figure 3A+B) and reduced the IC50 of INO by about 70% in both cell lines (from 0.676 nM to 0,221 nM and from 5.610 µM to 1.668 µM in 697 and NALM-6 cells, respectively).

To elucidate the underlying mechanism, comet assays under alkaline conditions were performed to assess DNA strand cleavage in cells pretreated with 1 µM BIRB 796 followed by INO exposure. Whereas INO alone causes low levels of DNA strand cleavage, the % DNA in tail almost doubled and increased from 20.1% (±7.7) to 36.7% (±13.3) for 697 cells and from 13.4% (±7.1) to 25.2% (±11.6) for NALM-6 cells in combination of INO with BIRB 796, respectively (Figure 3C+D). In addition, BIRB 796 elevated INO-induced γH2AX expression from 38.2% (±3.8) to 50.3% (±2.5) for 697 cells and from 45.7% (±4.6) to 62.2% (±0.9) for NALM-6 cells (Figure 3E+F), respectively.

Based on enhanced cytotoxicity, increased DNA fragmentation, and enhanced DDR signaling for the INO + BIRB 796 combination, we next analyzed the CAL + BIRB 796 combination in 697 and NALM-6 cells. BIRB 796 did enhance neither CAL- nor ETO- (Figure 3G-H and Supplemental Figure S3J-K) dependent cytotoxicity.

Complementary to pharmacological inhibition of p38 function, we analyzed the effects of reduced p38α expression using a stable CRISPR/Cas9-mediated knockdown. P38α-deficient cells exhibited a 40-50% reduction in cell growth compared to control cells. INO-induced p38 phosphorylation was markedly reduced following p38α knockdown. Similar to BIRB 796, depletion of p38α enhanced INO- but not CAL- induced cytotoxicity (Supplementary Figure S3L-S).

BIRB 796 enhances INO-induced mitochondrial priming and potentiates VEN-induced mitochondrial apoptosis

Mitochondrial priming describes different mitochondrial states to initiate apoptosis in response to defined signals such as exposure to BH3 mimetics (19, 20). To evaluate whether INO and BIRB 796 affect mitochondrial priming, 697 and NALM-6 cells were treated with INO or INO + BIRB 796 and then challenged with VEN to induce MOMP as described earlier (9). Cells were preincubated with INO or the combination of INO + BIRB 796, followed by the addition of 1 µM VEN for 3 h. Viable cells were analyzed by flow cytometry after TMRE staining. As shown in Figure 4 and supplemental Table 1, VEN induced MOMP as determined by reduction of mean fluorescence intensity (MFI) as compared to VEN-untreated controls. Preincubation with INO enhanced VEN-induced MOMP in a dose-dependent manner (Figure 4A+B), and BIRB 796 further augmented this effect at the INO concentration tested (34.7% (±4.3) to 45.5% (±2.8) for 697 cells and 61.1% (±3.5) to 73.3% (±1.7) for NALM-6 cells) (Figure 4C+D). After 24 h, the cytotoxic effects of the INO + VEN combination were enhanced by BIRB 796 (Figure 4E+F). Both the Chou-Talalay algorithm (data not shown) as well as Bliss analyses (Supplemental Figure S4A-D) revealed drug synergy of INO, VEN, and BIRB 796 with Bliss δ-scores between 11 and 34 in both cell lines.

INO, BIRB 796, and VEN exert synergistic cytotoxicity in high-risk BCP-ALL PDX cells

To translate these findings into clinically more relevant models, we used BCP-ALL patient-derived xenograft cells with different high-risk genetic aberrations (including TCF3::HLF, BCR::ABL1, and KMT2Ar) (Supplemental Table 2) in ex vivo cultures on human mesenchymal stromal cell layers for drug cytotoxicity studies.

In TCF3::HLF+ L707 PDX cells (t(17;19)) (15, 16) BIRB 796 effectively inhibited phosphorylation of p38 (Supplemental Figure S5A). Furthermore, co-treatment with INO and VEN enhanced cytotoxicity with synergistic Chou-Talalay (data not shown) and Bliss δ-scores for L707 and BCR::ABL1+ L4967 PDX cells (Figure 5A-D). The toxicity of INO + VEN was further increased by preincubation with BIRB 796, while the drug interaction remained highly synergistic (Figure 5E-H). This data was confirmed in four additional BCP-ALL PDX models with different genetic backgrounds, where the addition of BIRB 796 reduced IC50

concentrations for INO as well as INO+VEN combination therapy (Supplemental Figure S5B-C).

Since L707 cells co-express CD33, we differentially analyzed BIRB 796 in combination with INO, GO and CAL, respectively. As shown in Figure 5I-K, BIRB 796 significantly enhanced the cytotoxicity of INO and GO, but not of CAL, in a dose range of 10 to 500 pM. Similar data were found in a second BCP-ALL PDX model with co-expression of CD33 (Supplemental Figure S5D).

Triple combination therapy INO + BIRB 796 + VEN improves survival in murine t(17;19) PDX-ALL transplantation models

Based on these results, the triple combination was evaluated for clinically relevant endpoints in NSG mice engrafted with L707 cells in vivo. Since p38 inhibition seemed to increase CAL availability in INO + BIRB 796-treated cells, we designed a course of BIRB 796 and VEN (days 1-5) with two INO applications in cycle one, followed by a single INO application in cycles 2 and 3. BIRB 796 and VEN were administered p.o., whereas INO was given intravenously. Dosages were chosen with 10 mg/kg BIRB 796 and 20 mg/kg VEN, respectively, and 100 µg/kg for INO, equivalent to clinical dosages used in humans (7). Immunodeficient NSG mice were engrafted with luciferase-expressing L707 PDX cells (16) and were treated with 3 cycles of INO + BIRB-796 + VEN upon leukemic engraftment.

Leukemic burden and overall survival (OS) were monitored by bioluminescence (BLI) and Kaplan-Meier survival analysis, respectively (Figure 6). Study termination was defined at day 250. The control group showed a median survival of 23 days. All mice treated with INO + BIRB 796 or INO + VEN pharmacotherapy reached complete remission. Both dual combinations prolonged survival compared to controls and achieved an event-free survival rate of 20% (1 out of 5 mice) at day 250 (median survival: INO + VEN 70 days, INO + BIRB 796 83 days). In contrast, the triple combination markedly enhanced anti-leukemic efficacy and resulted in a long-term leukemia-free and overall survival rate of about 71% (5 out of 7 mice) at day 250 with a significant benefit for OS compared to dual therapy INO + VEN (Figure 6D). Cells isolated from the BM and spleen from relapse-free mice were analyzed, and no human CD19+ cells were detected.

To monitor in vivo side effects of pharmacotherapy, body weight and clinical scores were recorded for all mice. No clinical signs of toxicity were observed. The transient loss of body weight during the treatment period was most likely caused by the oral drug administration, as no significant differences in body weight loss were detected between the treatment groups. However, the body weight recovered after the end of drug treatment (Supplementary Figure S6A).

Analyses of relapsed L707 cells at the time mice were euthanized revealed human CD19 expression on more than 85% of cells harvested from BM and spleen (Supplementary Figure S6B). In addition, CD22 was expressed in all relapsed L707 PDX samples unchanged as compared to the initial leukemic graft despite prior VEN and INO treatment (Supplementary Figure S6C). Furthermore, MOMP induction upon ex vivo treatment with VEN showed no detectable difference compared to the initial L707 sample (Supplementary Figure S6D). Finally, INO-induced γH2AX signals were almost identical in both relapsed and initial L707 PDX cells (Supplementary Figure S6E).

Discussion

In our effort to optimize pharmacotherapy based on individual drug mechanisms of action, we molecularly analyzed INO, GO, CAL, BIRB 796 and VEN in BCP-ALL models, respectively.

CAL is among the most potent anti-tumor agents known to date, but most data on its activity were obtained from studies with plasmid DNA in vitro in the presence of strong reducing agents. We demonstrate CAL-induced DNA cleavage in viable BCP-ALL cells in a time-, dose-, and temperature-dependent manner (Figure 1B-D) in line with the need for adequate intracellular redox conditions for CAL activity in vivo (Figure 1E). In contrast to γ-irradiation and ETO, CAL induces DSBs at picomolar concentrations at a constant SSB:DSB ratio of about 3:1 (Figure 1F+G) (21). DSBs are considered more toxic than SSBs and potent inducers of apoptosis due to the difficulty of adequate DSB repair.

As compared to CAL, INO exhibits weaker DNA strand cleavage in alkaline comet assays and delayed onset of DDR signaling in line with intracellular processing and payload release kinetics (17). Besides different kinetics, higher molar concentrations of INO are required to achieve CAL-equivalent levels of apoptosis with a ratio of about 1:100 to 1:300. Fu et al. reported in general only about 2% of an ADC payload released and active inside the cell (22), corresponding to our functional data in both BCP-ALL cell lines. Obviously, linker chemistry plays a critical role in intracellular payload release. High linker stability minimizes systemic toxicity, but overly stable linkers can impair drug release and limit therapeutic efficacy (23).

INO and CAL induce identical DDR signaling intermediates, including phosphorylation of ATM, H2AX, and p38, as well as induction of p53 protein expression (Figure 2). These data suggest INO cytotoxicity is mainly or even exclusively dependent on CAL-induced DNA-strand cleavage. Furthermore, our results demonstrate an upstream position of ATM within the DDR signaling cascade with ATM-dependent phosphorylation of H2AX (γH2AX) and p38 as well as induction of p53 expression in response to INO treatment in BCP-ALL cells (Supplementary Figure S2) (24).

BIRB 796 is a potent inhibitor of p38α and p38β (and to a lesser extent p38γ/δ at higher concentrations) and blocks both p38 autophosphorylation and downstream kinase activity

(25). In BCP-ALL, p38 inhibition has been reported to suppress leukemic cell growth in vivo and to prolong survival in preclinical mouse models using BCP-ALL cell lines, underscoring its role as a pro-survival signal in ALL cells (13). In our study, pharmacological inhibition of p38 using BIRB 796 inhibited cell proliferation (Supplementary Figure S3D+E) and showed synergy with INO in several BCP-ALL cell lines and PDX cells irrespective of the cell's genetic aberrations (Figure 3A+B; Figure S5B). Furthermore, BIRB 796 enhanced INO-induced DNA fragmentation, DDR signaling, and cytotoxicity (Figure 3C-F). Interestingly, BIRB 796 enhances cytotoxicity of both INO and GO but not of CAL (Figure 5I-K), and cells with reduced p38α expression are more sensitive to INO but not to CAL treatment as compared to control cells (Supplementary Figure S3P-S). These data suggest that BIRB 796 cooperates with INO and GO upstream of DNA strand break induction and not on the level of INO- and CAL-induced DNA damage response signaling including p38 phosphorylation in BCP-ALL cells. Accordingly, the BIRB 796 – INO/GO interaction equals increasing CAL release from the respective ADC, and the underlying mechanisms may affect ADC internalization and/or linker cleavage, among others. A functional role of p38 for receptor endocytosis has been described for the EGFR upon phosphorylation of Ser1006 (26). However, endocytosis of Siglecs depends on tyrosine phosphorylation and their ITIM motifs (27-30), and a role of p38 for Siglec turnover has not yet been defined. In addition, since INO and GO share identical linkers for antibody-CAL coupling, BIRB 796 may also affect CAL release from the respective ADC. It is obviously of high scientific interest and translational relevance to further analyze the precise molecular mechanism of p38 interaction with Siglec-targeting ADCs in BCP-ALL and potentially AML as well.

The BH3 mimetic VEN displaces pro-apoptotic factors (e.g., BIM) from anti-apoptotic BCL2, thereby promoting MOMP (7, 9), and preliminary data from clinical studies with INO and VEN +/- Dexamethasone have recently been published (31, 32). In our study, INO induced mitochondrial priming in a dose-dependent manner that was further enhanced by co-treatment with BIRB 796 (Figure 4). MOMP induction by VEN after INO or INO + BIRB 796-mediated mitochondrial priming increased cytotoxicity in a synergistic manner in both BCP-ALL cell lines (Figure 4). In both cell lines and two BCP-ALL PDX models, the INO – VEN synergy is preserved in the presence of BIRB 796 in line with enhanced CAL availability upon BIRB 796 treatment. A triple combination therapy of INO + BIRB 796 + VEN was designed based on temporally modulating p38 signaling and mitochondrial priming in the critical therapeutic window of INO-induced DDR signaling. In NSG mice xenografted with luciferase-transduced L707 PDX cells, three cycles of INO + BIRB 796 + VEN or dual therapy with either INO + VEN or INO + BIRB 796 induced complete remission in all treated mice as assessed by BLI (Figure 6C). Dual combinations, however, resulted in long-term leukemia-free and overall survival in only 1 out of 5 mice (20%). These data are exactly in line with our previous report

for the INO + VEN + dexamethasone combination (7). In contrast, the triple combination of INO + BIRB 796 + VEN induced a long-term leukemia-free and overall survival in 5 out of 7 mice (71%) in the present study (Figure 6D). These data warrant clinical evaluation of this triple combination, especially in t(17;19)(q22;p13) BCP-ALL, currently considered not curable with chemotherapy.

When L707 PDX cells were analyzed upon relapses after prior therapy with INO, BIRB 796, and VEN for potential resistance mechanisms, we did not find relevant changes in CD19 or CD22 expression. In addition, MOMP induction by VEN or γH2AX induction by INO was not altered in relapsed L707 PDX cells as compared to the initial leukemic graft (Supplementary Figure S6). These data are in line with a previous study using different BCP-ALL PDX models and combined pharmaco- and immunotherapy using anti-CD19 CAR NK cells (33). These results may again suggest that relapses in these models may be due to protection of tumor cells during therapy (e.g., in some kind of “niches”) and subsequent expansion more than selection of drug-resistant (sub-) clones (34).

Several p38 inhibitors have already been evaluated in phase II clinical trials, e.g., losmapimod (GW856553) for muscular dystrophy, neflamapimod (VX-745) for neurodegenerative diseases, or talmapimod (SCIO-469) for multiple myeloma (11). For cancer treatment, ralimetinib, another p38α inhibitor, reached phase Ib/II trials for the treatment of ovarian cancer with gemcitabine and carboplatin and phase II trials for metastatic breast cancer in combination with tamoxifen. However, clinical inhibition of p38 seems to be difficult because of several side effects, including hepatotoxicity (35-37). BIRB 796, which was tested in this study, has been evaluated in inflammatory diseases and cancer and has been shown to enhance the effects of cytotoxic therapies in different tumor types (11, 38). BIRB 796 entered clinical trials (NCT02211157) but is also not further evaluated due to side effects such as hepatotoxicity (39).

These observations highlight the challenges of systemic p38 blockade because of its pleiotropic physiological roles (39, 40). To overcome these limitations, current strategies focus on more selective modulation, e.g., targeting the downstream kinase MK2, using PROTAC strategies to selectively degrade p38 isoforms, or preventing nuclear translocation of p38α (11). However, p38 inhibitors have been scheduled for longer periods in most studies, thereby potentially enhancing on- and off-target toxicities. In contrast, transient inhibition of p38 as used in our study may have therapeutic benefit in oncology. Our data suggests that short-term p38 inhibition may enhance tumor sensitivity to cytotoxic agents and Siglec-targeting ADCs in particular. Therefore, a short, pulse-like administration of p38 inhibitors could represent a rational strategy for combination therapies to potentiate anti-cancer efficacy while reducing cumulative systemic toxicities.

In conclusion, the combination of INO, BIRB 796, and VEN represents a mechanism-based strategy to overcome therapeutic resistance in BCP-ALL, including very high-risk BCP-ALL with t(17;19). Further preclinical and clinical evaluation is needed to refine this approach and improve therapeutic outcomes for patients with high-risk ALL.

References

1. Pui CH. Precision medicine in acute lymphoblastic leukemia. Front Med. 2020;14(6):689-700.
2. Kantarjian HM, DeAngelo DJ, Stelljes M, et al. Inotuzumab ozogamicin versus standard of care in relapsed or refractory acute lymphoblastic leukemia: Final report and long-term survival follow-up from the randomized, phase 3 INO-VATE study. Cancer. 2019;125(14):2474-2487.
3. Castaigne S, Pautas C, Terré C et al. Effect of gemtuzumab ozogamicin on survival of adult patients with de-novo acute myeloid leukaemia (ALFA-0701): a randomized, open-labeled, phase 3 study. Lancet. 2012;379(9825):1508-1516.
4. DiJoseph JF, Armellino DC, Boghaert ER, et al. Antibody-targeted chemotherapy with CMC-544: a CD22-targeted immunoconjugate of calicheamicin for the treatment of B-lymphoid malignancies. Blood. 2004;103(5):1807-1814.
5. Ellestad GA. Structural and conformational features relevant to the anti-tumor activity of calicheamicin gamma 1I. Chirality. 2011;23(8):660-6171.
6. Zein N, Sinha AM, McGahren WJ, Ellestad GA. Calicheamicin y1: An Antitumor Antibiotic That Cleaves Double-Stranded DNA Site Specifically. Science. 1988;240(4856):1198-1201.
7. Kirchhoff H, Karsli U, Schoenherr C, et al. Venetoclax and dexamethasone synergize with inotuzumab ozogamicin-induced DNA damage signaling in B-lineage ALL. Blood. 2021;137(19):2657-2661.
8. Souers AJ, Leverson JD, Boghaert ER, et al. ABT-199, a potent and selective BCL-2 inhibitor, achieves antitumor activity while sparing platelets. Nat Med. 2013;19(2):202-208.
9. Scherr M, Kirchhoff H, Battmer K, et al. Optimized induction of mitochondrial apoptosis for chemotherapy-free treatment of BCR-ABL+acute lymphoblastic leukemia. Leukemia. 2019;33(6):1313-1323.
10. Davids MS, Letai A. Targeting the B-cell lymphoma/leukemia 2 family in cancer. J Clin Oncol. 2012;30(25):3127-3135.
11. Canovas B, Nebreda AR. Diversity and versatility of p38 kinase signalling in health and disease. Nat Rev Mol Cell Biol. 2021;22(5):346-366.
12. Chang L, Karin M. Mammalian MAP kinase signalling cascades. Nature. 2001;410(6824):37-40.
13. Alsadeq A, Strube S, Krause S, et al. Effects of p38alpha/beta inhibition on acute lymphoblastic leukemia proliferation and survival in vivo. Leukemia. 2015;29(12):2307-2316.
14. Sarikidi A, Kefalakes E, Falk CS, et al. Altered Immunomodulatory Responses in the CX3CL1/CX3CR1 Axis Mediated by hMSCs in an Early In Vitro SOD1(G93A) Model of ALS. Biomedicines. 2022;10(11):2916.

15. Pal D, Blair HJ, Elder A, et al. Long-term in vitro maintenance of clonal abundance and leukaemia-initiating potential in acute lymphoblastic leukaemia. Leukemia. 2016;30(8):1691-1700.
16. Bomken S, Buechler L, Rehe K, et al. Lentiviral marking of patient-derived acute lymphoblastic leukaemic cells allows in vivo tracking of disease progression. Leukemia. 2013;27(3):718-721.
17. de Vries JF, Zwaan CM, De Bie M, et al. The novel calicheamicin-conjugated CD22 antibody inotuzumab ozogamicin (CMC-544) effectively kills primary pediatric acute lymphoblastic leukemia cells. Leukemia. 2012;26(2):255-264.
18. Olive PL, Banath JP. The comet assay: a method to measure DNA damage in individual cells. Nat Protoc. 2006;1(1):23-29.
19. Potter DS, Letai A. To Prime, or Not to Prime: That Is the Question. Cold Spring Harb Symp Quant Biol. 2016;81:131-140.
20. Singh R, Letai A, Sarosiek K. Regulation of apoptosis in health and disease: the balancing act of BCL-2 family proteins. Nat Rev Mol Cell Biol. 2019;20(3):175-193.
21. Muslimovic A, Nystrom S, Gao Y, Hammarsten O. Numerical analysis of etoposide induced DNA breaks. PLoS One. 2009;4(6):e5859.
22. Fu Z, Li S, Han S, Shi C, Zhang Y. Antibody drug conjugate: the "biological missile" for targeted cancer therapy. Signal Transduct Target Ther. 2022;7(1):93.
23. Beck A, Goetsch L, Dumontet C, Corvaia N. Strategies and challenges for the next generation of antibody-drug conjugates. Nat Rev Drug Discov. 2017;16(5):315-337.
24. Blackford AN, Jackson SP. ATM, ATR, and DNA-PK: The Trinity at the Heart of the DNA Damage Response. Mol Cell. 2017;66(6):801-817.
25. Kuma Y, Sabio G, Bain J, et al. BIRB796 inhibits all p38 MAPK isoforms in vitro and in vivo. J Biol Chem. 2005;280(20):19472-19479.
26. Perez Verdaguer M, Zhang T, Paulo JA, et al. Mechanism of p38 MAPK-induced EGFR endocytosis and its crosstalk with ligand-induced pathways. J Cell Biol. 2021;220(7):e202102005.
27. Crocker PR, Varki A. Siglecs in the immune system. Immunology. 2001;103(2):137-145.
28. Laubli H, Nalle SC, Maslyar D. Targeting the Siglec-Sialic Acid Immune Axis in Cancer: Current and Future Approaches. Cancer Immunol Res. 2022;10(12):1423-1432.
29. John B, Herrin BR, Raman C, et al. The B cell coreceptor CD22 associates with AP50, a clathrin-coated pit adapter protein, via tyrosine-dependent interaction. J Immunol. 2003;170(7):3534-3543.

30. Walter RB, Raden BW, Zeng R, Bernstein ID, Cooper JA. ITIM-dependent endocytosis of CD33-related Siglecs: role of intracellular domain, tyrosine phosphorylation, and the tyrosine phosphatases, Shp1 and Shp2. J Leukoc Biol. 2008;83(1):200-211.
31. Luskin M, Keating J, Frost B, et al. Venetoclax plus inotuzumab ozogamicin for relapsed and refractory ALL: Results of a phase I trial. Blood. 2025;146(Supplement 1):645.
32. Wan Z, Ji Y, Lou D, et al. Efficacy and safety of inotuzumab ozogamicin combined with venetoclax and dexamethasone in relapsed/refractory B-cell acute lymphoblastic leukemia (R/R B-ALL). Blood. 2025;146(Supplement 1):1569.
33. Kirchhoff H, Schoenherr C, Fleischer L, et al. Combination of targeted pharmacotherapy and immunotherapy with anti-CD19 CAR NK cells in acute lymphoblastic leukemia. Hemasphere. 2025;9(10):e70238.
34. Ebinger S, Ozdemir EZ, Ziegenhain C, et al. Characterization of Rare, Dormant, and Therapy-Resistant Cells in Acute Lymphoblastic Leukemia. Cancer Cell. 2016;30(6):849-862.
35. Martinez-Limon A, Joaquin M, Caballero M, Posas F, de Nadal E. The p38 Pathway: From Biology to Cancer Therapy. Int J Mol Sci. 2020;21(6):1913.
36. Patnaik A, Haluska P, Tolcher AW, et al. A First-in-Human Phase I Study of the Oral p38 MAPK Inhibitor, Ralimetinib (LY2228820 Dimesylate), in Patients with Advanced Cancer. Clin Cancer Res. 2016;22(5):1095-1102.
37. Vergote I, Heitz F, Buderath P, et al. A randomized, double-blind, placebo-controlled phase 1b/2 study of ralimetinib, a p38 MAPK inhibitor, plus gemcitabine and carboplatin versus gemcitabine and carboplatin for women with recurrent platinum-sensitive ovarian cancer. Gynecol Oncol. 2020;156(1):23-31.
38. He D, Zhao XQ, Chen XG, et al. BIRB796, the inhibitor of p38 mitogen-activated protein kinase, enhances the efficacy of chemotherapeutic agents in ABCB1 overexpression cells. PLoS One. 2013;8(1):e54181.
39. Zheng Q, Li S, Wang A, et al. p38 mitogen-activated protein kinase: Functions and targeted therapy in diseases. MedComm Oncol. 2023;2(3):e53.
40. Garcia-Hernandez L, Garcia-Ortega MB, Ruiz-Alcala G, Carrillo E, Marchal JA, García MA. The p38 MAPK Components and Modulators as Biomarkers and Molecular Targets in Cancer. Int J Mol Sci. 2021;23(1):370.

Figure Legends

Figure 1. Inotuzumab ozogamicin (INO)- and calicheamicin (CAL)-mediated DNA strand breaks in alkaline and neutral comet assays. (A) 697 cells were incubated with IC50 of INO (697: 660 pM) for 6 h or with IC50 of CAL (697: 7.5 pM) for 2 h. **(B+C)** 697 cells were treated with 500 pM CAL for 10 to 60 min, with representative microscope images of CAL-treated cells shown in (B). **(D)** 697 cells were treated with increasing CAL concentrations for 30 min or **(E)** with 250 pM CAL for 30 min at 37 °C and 4 °C. **(F+G)** Comparison of DNA strand breaks induced in 697 cells by γ-irradiation (6 Gy), etoposide (ETO) (5 µM), and CAL (1 nM) after 30 min. Cells were analyzed in comet assays under alkaline (A-F) or neutral conditions (G). Each symbol represents one cell, with n=65 cells examined for each experimental condition. *p<0.05, **p<0.01, ****p<0.0001, determined using the Kruskal-Wallis test and subsequent Dunn's multiple comparison test.

Figure 2: DNA damage response (DDR) kinetics after CAL and INO treatment. 697 cells were treated with their IC50 of CAL (7.5 pM) and INO (0.66 nM). The protein expression of pATM, γH2AX, pp38, p38α, p53, and cleaved PARP1 in Western blot was quantified and normalized to GAPDH.

Figure 3: BIRB 796 potentiates INO-mediated cytotoxicity and DNA damage signaling. (A+B) 697 (A) and NALM-6 cells (B) were pretreated for 24 h with 1 µM BIRB 796, following treatment with increasing concentrations of INO for 24 h. Apoptotic cells were detected using PI staining (n=3). **(C+D)** 697 (C) and NALM-6 cells (D) were pretreated for 1 h with 1 µM BIRB 796 followed by incubation with 3.3 nM INO for 8 h. Cells were analyzed in comet assays under alkaline conditions with n=65 cells examined for each experimental condition. The results from three independent experiments are shown. **(E+F)** 697 (E) and NALM-6 cells (F) were pretreated for 24 h with 1 µM BIRB 796, following treatment with INO (697: 0.66 nM, NALM-6: 6.6 nM) for 6 h. Cells were fixed and stained with anti-γH2AX antibody (n=4). **(G+H)** 697 (G) and NALM-6 (H) cells were pretreated for 24 h with 1 µM BIRB 796, following treatment with increasing concentrations of CAL for 24 h. Apoptotic cells were detected using PI staining (n=3). ***p<0.001, ****p<0.0001, determined using the one-way (E+F) or two-way ANOVA (A+B+G+H) with the Bonferroni's post hoc test or Kruskal-Wallis test and subsequent Dunn's multiple comparison test (C+D).

Figure 4: BIRB 796 potentiates INO-induced mitochondrial priming and enhances venetoclax (VEN)-induced mitochondrial apoptosis. (A+B) 697 (A) and NALM-6 cells (B) were pretreated with increasing concentrations of INO for 21 h and subsequently incubated

with 1 µM VEN for 3 h. Cells were stained with TMRE for 20 min. **(C+D)** Cells were pretreated with 1 µM BIRB 796 for 24 h, followed by INO treatment (697: 0.033 nM, NALM-6: 0.165 nM) for an additional 21 h. Cells were then incubated with VEN for 3 h and stained with TMRE for 20 min. (A-D) Cells were analyzed by flow cytometry. The reduction of mean TMRE fluorescence (%) is shown relative to controls without VEN treatment (n=4**). (E+F)** 697 (E) and NALM-6 cells (F) were treated in the presence or absence of a 24 h pre-treatment with 1 µM BIRB, alone or in combination with fixed ratios of INO and VEN for 24 h. Apoptotic cells were detected using PI staining and flow cytometry analysis (n=3). **p<0.01, ***p<0.001, ****p<0.0001, p-values were calculated by one-way (A+B) or two-way ANOVA (C+D) with the Bonferroni's post hoc test.

Figure 5: BIRB 796 enhances INO-induced cytotoxicity in L707 and L4967 patient-derived xenograft (PDX) cells. (A-H) L707 (A,C,E,G) and L4967 PDX cells (B,D,F,H) were cultured on human MSCs and were treated in the absence (A-D) or presence (E-H) of a 4 h (L707) or 24 h (L4967) pre-treatment with 10 µM BIRB, alone or in combination with fixed ratios of INO and VEN for 48 h (n=3). (A,B,E,F) Relative cell viability as detected by PI/CalceinAM staining and flow cytometry analysis (n=3). (C,D,G,H) calculated Bliss Scores. **(I-K)** L707 PDX cells were cultured on MSCs and pretreated with 10 µM BIRB 796 for 4 h or 24 h, followed by an incubation with increasing concentrations of (I) INO, (J) gemtuzumab ozogamicin (GO) or (K) CAL for 48 h. Apoptotic cells were detected using PI/CalceinAM staining and flow cytometry analysis (n=3). ***p<0.001, ****p<0.0001, p-values were calculated by two-way ANOVA with the Bonferroni's post hoc test.

Figure 6: Treatment of NSG mice with combination therapy of INO (I), BIRB 796 (B), and VEN (V). NSG mice were transplanted intravenously with $1x10^6$ L707 PDX cells, which were stably transduced with luciferase. Tumor growth was monitored using non-invasive bioluminescence imaging (BLI) via luciferase reporter expression. Mice were randomly assigned to treatment groups after confirmed engraftment of leukemia on day 13 after transplantation. This was followed by three weeks of therapy with VEN (20 mg/kg) and BIRB 796 (10 mg/kg) via oral gavage on 5 days per week. INO (100 µg/kg) was injected intravenously twice in therapy week one and once in each therapy week 2 and 3. **(A)** Representative BLI for one mouse per treatment group. **(B+C)** BLI signals (total flux) were analyzed at the start (B) and end (C) of therapy and were quantified using Living Image 4.7.4 software. **(D)** Kaplan-Meier overall survival (OS) curve of L707 mice. *p<0.05, **p<0.01, ***p<0.001, p-values were calculated by log-rank test.

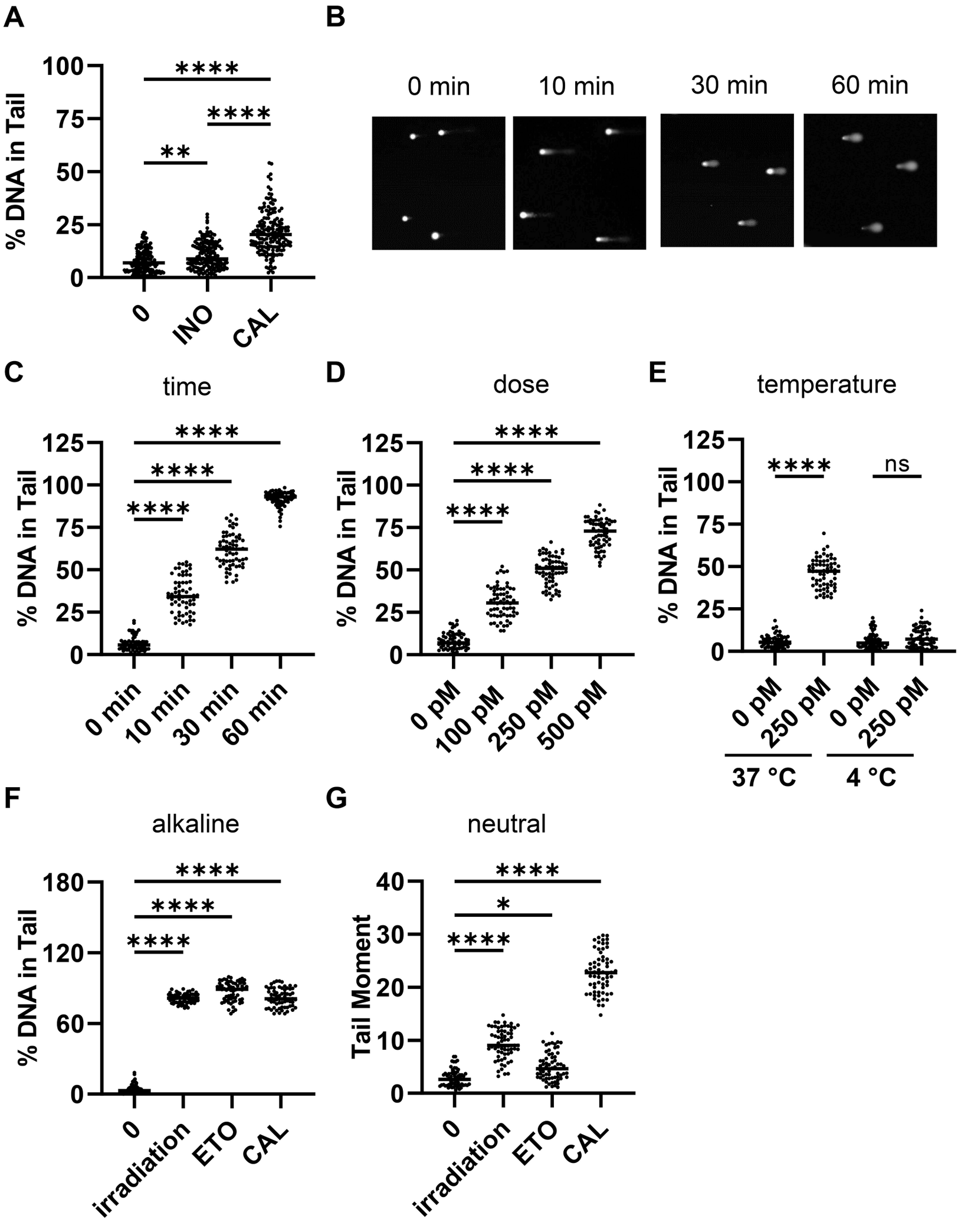
A
% DNA in Tail
100
75
50
25
0
****
****
**
0
INO
CAL
B
0 min
10 min
30 min
60 min
C
time
% DNA in Tail
125
100
75
50
25
0
****
****
****
0 min
10 min
30 min
60 min
D
dose
% DNA in Tail
125
100
75
50
25
0
****
****
****
0 pM
100 pM
250 pM
500 pM
E
temperature
% DNA in Tail
125
100
75
50
25
0
****
ns
0 pM
250 pM
0 pM
250 pM
37 °C
4 °C
F
alkaline
% DNA in Tail
180
120
60
0
****
****
****
0
irradiation
ETO
CAL
G
neutral
Tail Moment
40
30
20
10
0
****
*
****
0
irradiation
ETO
CAL

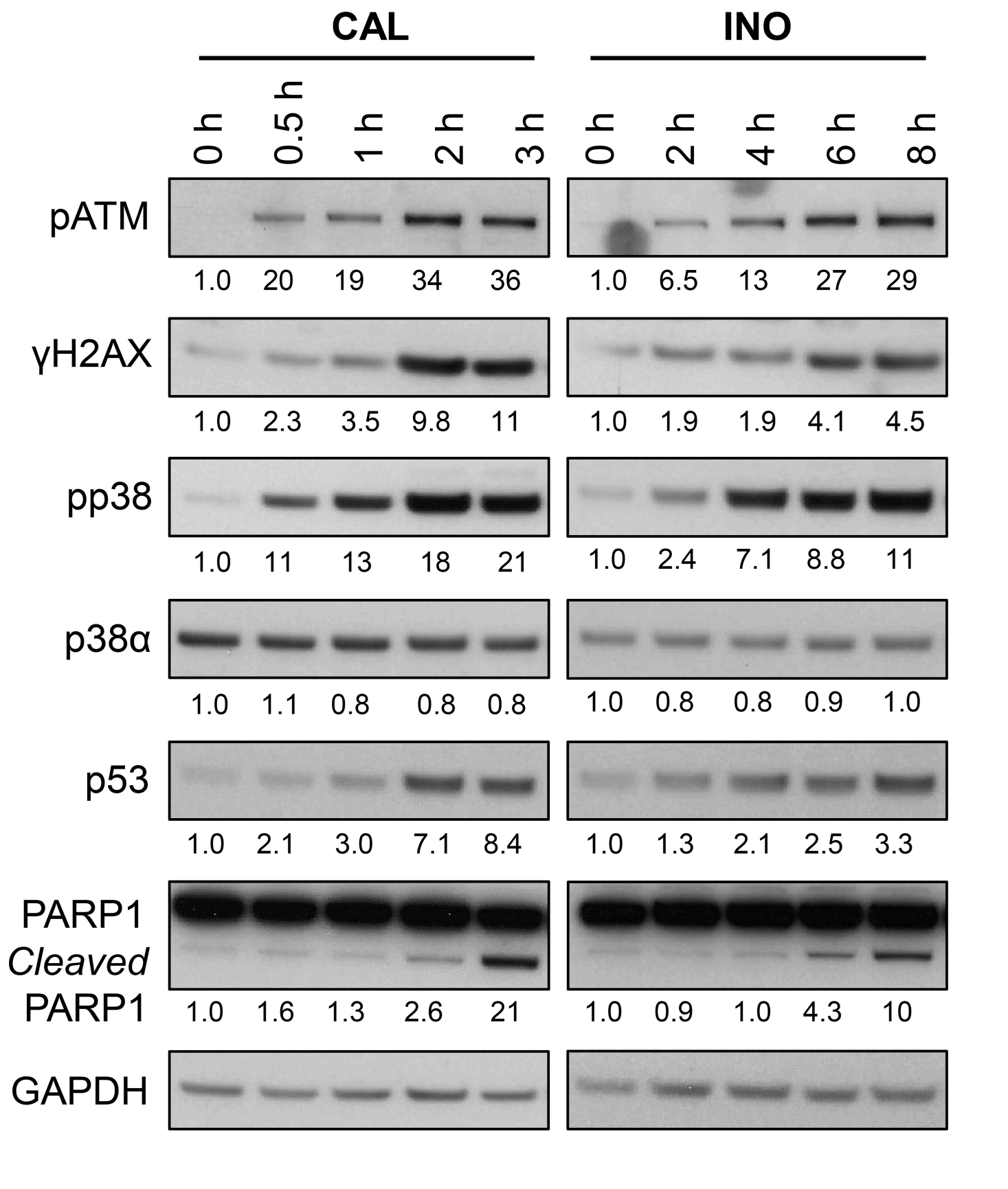
CAL
INO
0 h
0.5 h
1 h
2 h
3 h
0 h
2 h
4 h
6 h
8 h
pATM
1.0 20 19 34 36
1.0 6.5 13 27 29
γH2AX
1.0 2.3 3.5 9.8 11
1.0 1.9 1.9 4.1 4.5
pp38
1.0 11 13 18 21
1.0 2.4 7.1 8.8 11
p38α
1.0 1.1 0.8 0.8 0.8
1.0 0.8 0.8 0.9 1.0
p53
1.0 2.1 3.0 7.1 8.4
1.0 1.3 2.1 2.5 3.3
PARP1
Cleaved
PARP1
1.0 1.6 1.3 2.6 21
1.0 0.9 1.0 4.3 10
GAPDH

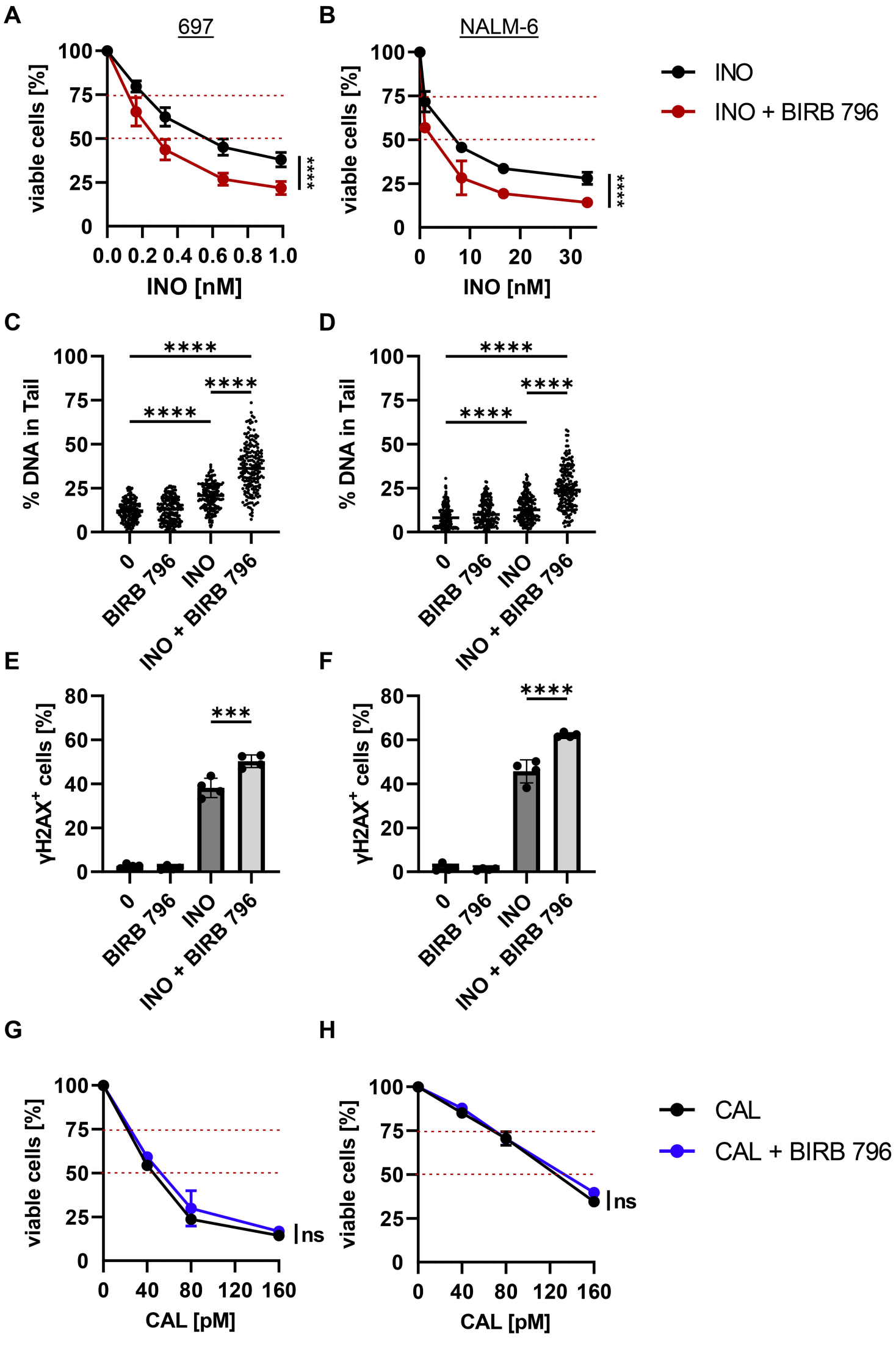
A
697
viable cells [%]
INO [nM]
****
B
NALM-6
viable cells [%]
INO [nM]
****
INO
INO + BIRB 796
C
% DNA in Tail
****
****
****
0
BIRB 796
INO
INO + BIRB 796
D
% DNA in Tail
****
****
****
0
BIRB 796
INO
INO + BIRB 796
E
γH2AX+ cells [%]
***
0
BIRB 796
INO
INO + BIRB 796
F
γH2AX+ cells [%]
****
0
BIRB 796
INO
INO + BIRB 796
G
viable cells [%]
CAL [pM]
ns
H
viable cells [%]
CAL [pM]
ns
CAL
CAL + BIRB 796

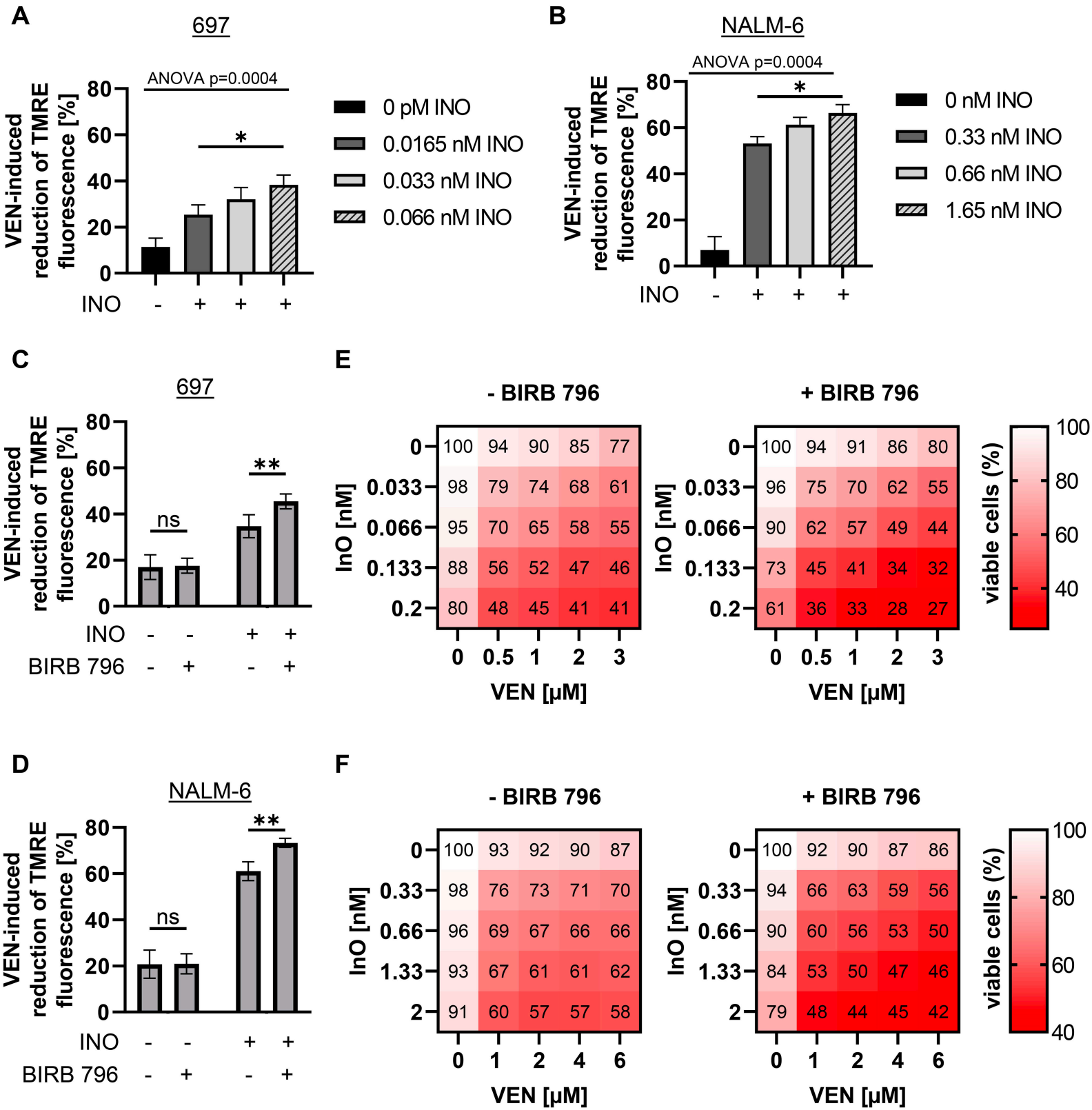
A
697
ANOVA p=0.0004
VEN-induced reduction of TMRE fluorescence [%]
INO
0 pM INO
0.0165 nM INO
0.033 nM INO
0.066 nM INO
B
NALM-6
ANOVA p=0.0004
0 nM INO
0.33 nM INO
0.66 nM INO
1.65 nM INO
C
697
ns
**
BIRB 796
D
NALM-6
E
- BIRB 796
+ BIRB 796
InO [nM]
VEN [µM]
viable cells (%)
F

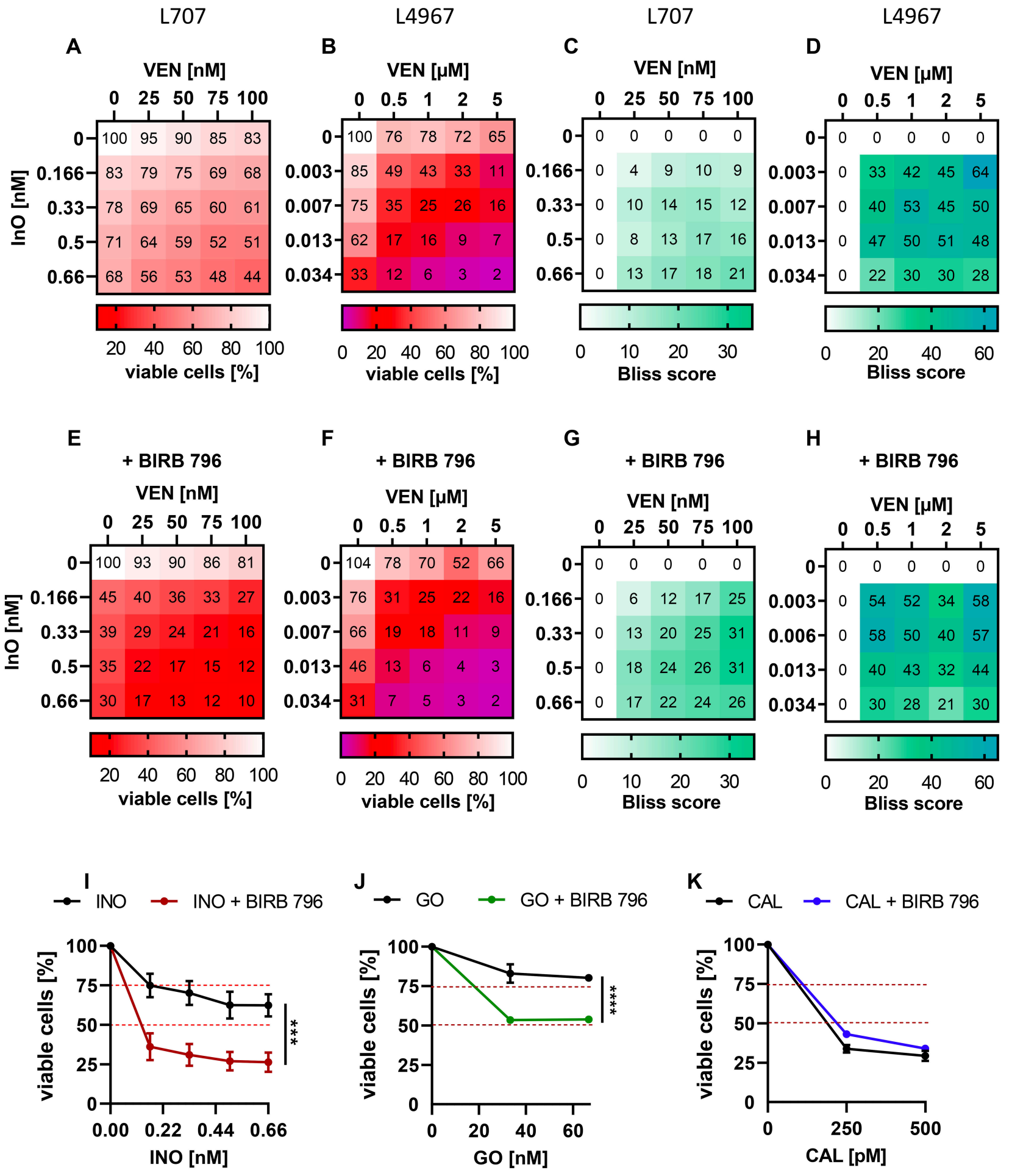
L707
L4967
L707
L4967
A
B
C
D
VEN [nM]
VEN [µM]
InO [nM]
viable cells [%]
Bliss score
+ BIRB 796
E
F
G
H
I
J
K
INO
INO + BIRB 796
GO
GO + BIRB 796
CAL
CAL + BIRB 796
INO [nM]
GO [nM]
CAL [pM]
***
****

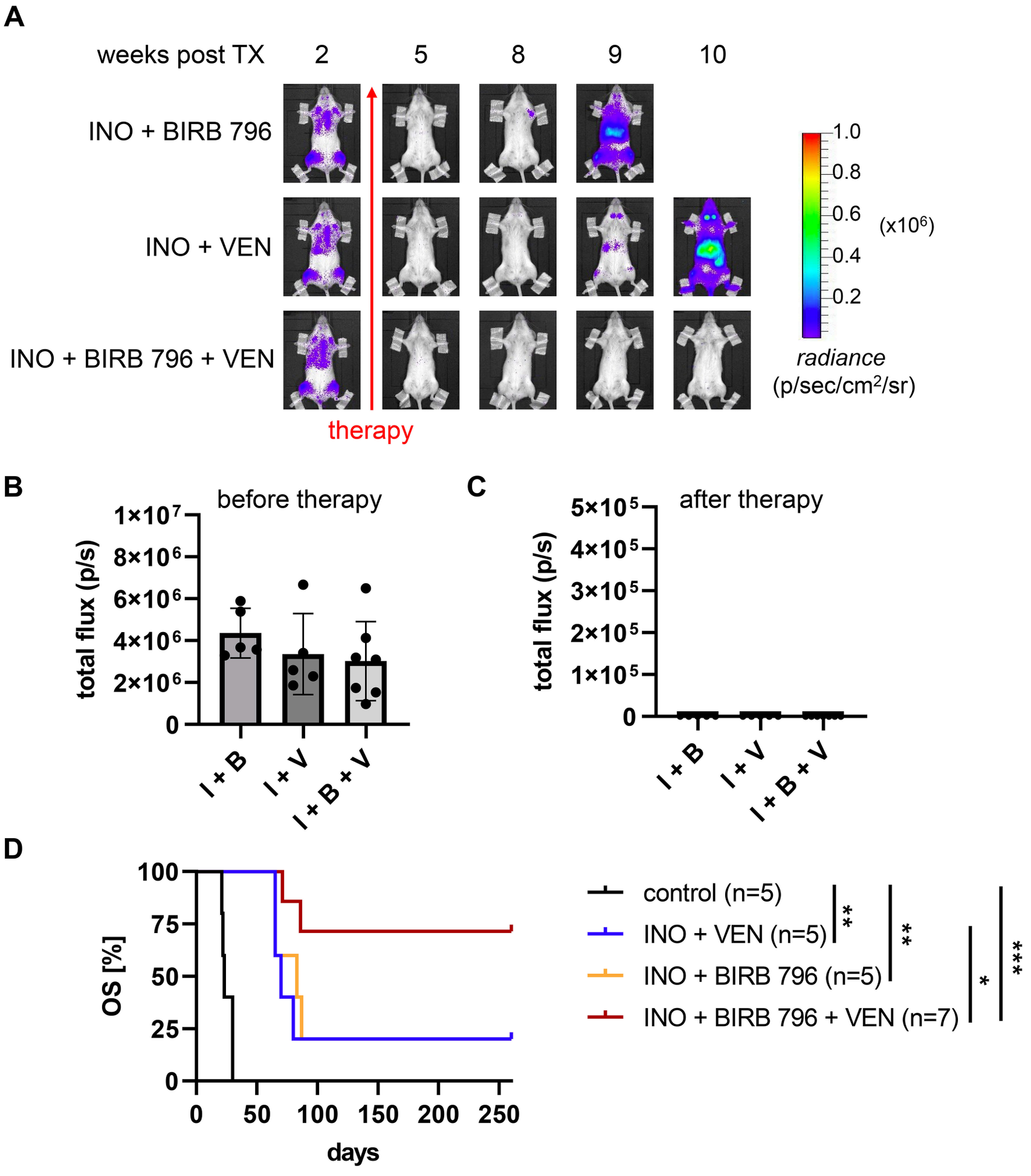
A
weeks post TX
2
5
8
9
10
INO + BIRB 796
INO + VEN
INO + BIRB 796 + VEN
therapy
1.0
0.8
0.6
0.4
0.2
(x10⁶)
radiance
(p/sec/cm²/sr)
B
before therapy
total flux (p/s)
1×10⁷
8×10⁶
6×10⁶
4×10⁶
2×10⁶
0
I + B
I + V
I + B + V
C
after therapy
total flux (p/s)
5×10⁵
4×10⁵
3×10⁵
2×10⁵
1×10⁵
0
I + B
I + V
I + B + V
D
OS [%]
100
75
50
25
0
0
50
100
150
200
250
days
control (n=5)
INO + VEN (n=5)
INO + BIRB 796 (n=5)
INO + BIRB 796 + VEN (n=7)
**
**
*
***

Supplementary Material and Methods

Pharmacologic agents

For ex vivo studies, VEN, KU-60019, and BIRB 796 were purchased from Selleck Chemicals (Houston, TX, USA) and solubilized in dimethyl sulfoxide (DMSO) (Merck, Darmstadt, Germany) to 10 mM stocks. INO and GO (Pfizer, New York, NY, USA) were dissolved in 0.9% NaCl (BD Bioscience, San Jose, CA, USA) at 0.25 mg/ml and 1 mg/ml concentration, respectively. The pharmacologic agents were supplemented to the culture medium at the required concentrations. For in vivo studies, VEN was solubilized in a vehicle consisting of 60% phosal, 30% PEG 400, and 10% ethanol (all from Sigma-Aldrich, St. Louis, MO, USA). BIRB 796 (MedChemExpress, Monmouth Junction, NJ, USA) was applied in 5% DMSO, 40% PEG 400, 5% TWEEN 20 (Sigma-Aldrich, St. Louis, MO, USA), and 50% water.

Cell lines

The BCP-ALL cell lines 697 and NALM-6 (DSMZ, Braunschweig, Germany) (1, 2) were cultured in RPMI 1640 (Gibco, Grand Island, NY, USA) supplemented with 10% FCS (Sigma-Aldrich, St. Louis, MO, USA) and 1% penicillin/streptomycin (P/S) (Gibco, Grand Island, NY, USA). 293T cells (DSMZ, Braunschweig, Germany) were used for lentivirus production and were cultured in DMEM (Gibco, Grand Island, NY, USA) supplemented with 10% FCS and 1% P/S.

Construction of lentiviral vectors

shRNAs of the human *ATM* gene (GeneBank accession no. NM_000051.4; targeting sequence 5' GGATTTGCGTATTACTCAG 3'), lentiviral transgene plasmids pdc-SEW, and shRNA controls were cloned as previously described (3, 4). For CRISPR/Cas9-mediated gene knockdown, guide RNAs of the human p38α MAPK14 gene (GeneBank accession no. NM_001315.3; targeting sequence 5' CACAAAAACGGGGTTACGTG 3') were cloned, following the protocol of the Zhang Lab (5, 6).

Lentiviral constructs, containing the shRNAs or guide RNAs, encode green fluorescent protein (GFP) as a reporter gene. Oligonucleotides were purchased from BioSpring (Frankfurt, Germany) and solubilized in 100 µM stocks in water. The preparation of recombinant lentiviral supernatants and lentiviral transductions were performed as described earlier (3, 7) Transduction efficacy was assessed by GFP expression using a FACS Calibur with CellQuest Pro software version 4.0.2 (both BD Bioscience, San Jose, CA, USA).

Drug treatment and assessment of cytotoxicity

For the assessment of IC50 concentrations of INO and CAL, cell lines were treated with increasing concentrations of cytotoxic agents for 24 h. For combination treatment studies, cell

lines were incubated with 1 µM BIRB 796 in combination with increasing concentrations of INO and VEN, either alone or in fixed ratios. Cytotoxicity was assessed by staining with 10 µg/ml PI. Cells were analyzed in a FACS Calibur and with the CellQuest Pro software version 4.0.2. PDX cells were seeded $1x10^6$/ml in SFEM II medium (Stemcell technologies, Cambridge, UK) supplemented with 20% FCS, 1% Pen/Strep, 20ng/ml recombinant IL-3 and 10ng/ml recombinant IL-7 (Peprotech, Hamburg, Germany) on MSCs in the absence or presence of 10 µM BIRB 796. After preincubation for 4-24 h the respective drugs were added for 48 hours followed by Calcein AM/PI staining. Cells were analyzed in a FACS Calibur and with the CellQuest Pro software version 4.0.2 or with a CytoFLEX and CytExpert software version 1.2 (Beckman Coulter, Brea CA, USA).

For analysis of drug synergy CI values were calculated using CompuSyn software version 1.0 (8) and Bliss scores were calculated using SynergyFinder 3.0 (9).

MOMP induction

Cells were pretreated with INO and/or BIRB 796 for 24 h at a cell density of $0.5x10^6$ cells/ml in 6-well plates. Subsequently, cells were counted again and incubated for 3 h with 1 µM VEN at a cell density of $0.5x10^6$ cells/ml in FACS tubes at 37 °C. MOMP assessment was performed as described (10).

Detection of intracellular γH2AX and pATM expression

After 6 h of INO treatment, cells were fixed with 4% paraformaldehyde (Thermo Fisher Scientific, Waltham, MA, USA) for 15 min at 4 °C. Cells were washed in PBS, and cell pellets were resuspended in ice-cold methanol and stored at -20 °C. For detection of intracellular γH2AX and pATM expression, cells were washed with PBS, followed by staining with anti-γH2AX (pSer139) antibody (#560443, BD Bioscience, San Jose, CA, USA) or anti-pATM (pSer1981) (#81292, Abcam, Cambridge, UK) for 1 h at room temperature (RT) in PBS. Cells were washed with PBS and incubated with APC-conjugated anti-mouse antibody (BD Bioscience, San Jose, CA, USA) for 30 min. Cells were washed and resuspended in PBS and analyzed in a FACS Calibur flow cytometer.

Immunoblotting

Whole cell lysates were prepared in lysis buffer (20 mM HEPES, pH 7.5, 0.4 M NaCl, 1 mM EDTA, 1 mM EGTA (both Serva, Heidelberg, Germany), 1 mM DTT (Sigma-Aldrich, St. Louis, MO, USA)) supplemented with mini complete protease inhibitor cocktail tablet (Roche Diagnostics, Mannheim, Germany), mixed with NuPAGE loading buffer (Invitrogen, Waltham, MA, USA), sonicated, and boiled at 96 °C for 5 min.

Lysates were separated by sodium dodecyl sulfate polyacrylamide gel electrophoresis (SDS-PAGE) and transferred to Hybond enhanced chemiluminescence (ECL) nitrocellulose membrane (Thermo Fisher Scientific, Waltham, MA, USA). Membranes were incubated with the following antibodies according to the manufacturer's protocol: anti-ATM (CS2873), anti-pATM (Ser1981) (CS4526), anti-GAPDH (CS2118), anti-γH2AX (Ser139) (BD 560443), anti-p38α (CS9218), anti-pp38 (Thr180/Tyr182) (CS4511), anti-p53 (sc-126), and anti-PARP1 (CS9532). Chemiluminescence was used for visualization using the ECL Western blotting detection reagents (Revvity, Waltham, MA, USA) according to manufacturer instructions. Densitometric analysis of x-ray films was performed using Fiji software. The intensity ratio of the protein of interest band to the GAPDH band as a loading control was calculated.

Comet Assay

After exposure to DNA-damaging agents, cells were suspended in cold PBS at cell density of 10^5 cells/ml, mixed with molten low-melting agarose in a ratio of 1:10, and spread onto *CometSlides*. Slides were immersed in the *CometAssay* lysis solution overnight at 4 °C.

For the comet assay under alkaline conditions, the cells were denatured for 1 h in alkaline solution (200 mM NaOH, 1 mM EDTA) at RT. After electrophoresis at 4 °C for 1 h at 20 V in alkaline solution, slides were washed twice for 5 min in water and then for 5 min in 70% ethanol. For the comet assay under neutral conditions, the slides were immersed in neutral electrophoresis solution (50 mM Tris, 150 mM sodium acetate) for 30 min after lysis, followed by electrophoresis at 4 °C for 1 h at 20 V. Cells were incubated for 30 min with DNA precipitation solution (1 M ammonium acetate, 80% ethanol), followed by a further incubation for 30 min in 70% ethanol at RT. The slides from alkaline or neutral treatment were then dried at 37 °C for 15 min and stained with 100 µl of 1X SYBR Gold solution (Invitrogen, Waltham, MA, USA). Comet images were taken with an Axiovert 200 M microscope using AxioVision 4.8 software (both from Carl Zeiss, Jena, Germany) and analyzed with Comet Assay IV Software (Instem, Stone, Staffordshire, UK) by calculation of % DNA in tail for alkaline comet assay or tail moment (% DNA in tail x tail length) for neutral comet assay.

PDX cells and animal experiments

Primary peripheral blood or bone marrow samples from BCP-ALL patients were used in accordance with the Declaration of Helsinki after written informed consent of the respective patients and with approval from the ethical committee of Hannover Medical School for studies involving human blood or bone marrow (8345_BO_S_2019). BCP-ALL PDX models were generated using tail vein injection of primary samples in NSG mice as previously described (10). When engrafted mice showed signs of leukemia, animals were euthanized and PDX cells were harvested from bone marrow and spleen.

For bioluminescence imaging analyses, D-luciferin (1 mg/mouse) (AppliChem, Darmstadt, Germany) was applied intraperitoneally, and the imaging of tumor growth was detected by using IVIS Lumina II (Caliper Life Sciences, Hopkinton, MA, USA). Living Image 4.7.4 software was used to analyze the bioluminescence radiance. Mice were randomly allocated to each group and treated with the respective antineoplastic agents for three weeks. BIRB 796 (10 mg/kg) was applied by oral gavage 5 days per week in combination with VEN (20 mg/kg) with a treatment delay of a minimum of 2 h. INO was administered intravenously at a dose of 100 µg/kg in 0.9% NaCl twice during the first week (day 2 and day 5 of the treatment period) and once per week (day 3) during the second and third week of the treatment period. Treatment-related toxicity was determined by daily evaluation of body weight, visual appearance, and cage activity during the pharmacological treatment period. All animal studies were in accordance with the German animal protection law and with the European Communities Council Directive 86/609/EEC and 2010/63/EU for the protection of animals used for experimental purposes. All experiments were approved by the Local Institutional Animal Care and Research Advisory Committee and permitted by the local authority, the Lower Saxony State Office for Consumer Protection and Food Safety (LAVES) (No. 33.14-42502-04 -19/3217 and No. 33.12-42502-04-21/3711).

Analysis of relapsed PDX samples

PDX cells of relapsed mice were isolated from the spleen and bone marrow (BM). Cells were stained with anti-huCD19-APC, anti-huCD45-FITC, and anti-huCD22-APC antibodies (all from BioLegend, San Diego, CA, USA) for 20 min at RT. For functional analysis, MOMP induction by VEN and γH2AX induction by INO were analyzed as described earlier.

Statistical Analysis

All data are presented as mean ± SD unless otherwise indicated. Statistical analyses were performed using GraphPad Prism software version 9.5.0 (GraphPad Software, San Diego, CA, USA). To assess the statistical significance of the results, one-way or two-way ANOVA with Bonferroni correction for multiple group comparisons was used. For non-parametric data, the Kruskal-Wallis test with Dunn's post hoc multiple comparison was applied. Survival analyses were conducted using the Kaplan-Meier method and compared by log-rank test. P-values < 0.05 were considered significant.

Supplementary Table 1

697	3 hours treatment							
	untreated				VEN			
pretreatment (20 hours)	Mean (±SD)	n=1	n=2	n=3	Mean (±SD)	n=1	n=2	n=3
none	**652.7 (±40.9)**	694.4	612.6	651.2	**579.5 (±60.8)**	638.4	517.0	583.0
0.0165nM INO	**713.6(±62.5)**	777.6	652.6	710.7	**516.4 (±32.7)**	549.2	516.1	483.8
0.033nM INO	**792.8(±142.1)**	909.7	634.7	834.0	**535.6 (±80.5)**	621.9	462.5	522.4
0.066nM INO	**839.6(±165.5)**	1025.7	709.0	783.9	**513.6 (±65.3)**	588.2	466.8	485.8

NALM-6	3 hours treatment							
	untreated				VEN			
pretreatment (20 hours)	Mean (±SD)	n=1	n=2	n=3	Mean (±SD)	n=1	n=2	n=3
none	**674.4 (±160.5)**	599.7	564.9	858.6	**604.0 (±159.7)**	527.1	497.3	787.6
0.33nM INO	**749.9 (±158.0)**	642.8	675.4	931.4	**352.4 (±84.6)**	314.5	293.3	449.3
0.66nM INO	**726.2 (±119.1)**	667.1	648.2	863.4	**282.1 (±61.8)**	270.0	227.3	349.2
1.65nM INO	**638.2 (±110.4)**	658.5	519.0	737.1	**216.8 (±58.7)**	222.0	155.7	272.8

697	3 hours treatment									
	untreated					VEN				
pretreatment (20 hours)	Mean (±SD)	n=1	n=2	n=3	n=4	Mean (±SD)	n=1	n=2	n=3	n=4
none	**794.6 (±117.7)**	640.0	807.0	805.0	926.5	**619.6 (±95.5)**	581.0	521.4	629.5	746.7
INO	**839.5 (±135.6)**	667.1	810.4	986.5	894.1	**543.8 (±56.0)**	485.5	513.9	612.5	563.4
BIRB 796	**835.9 (±77.2)**	725.6	855.4	857.0	905.7	**689.6 (±76.8)**	586.0	677.3	741.5	753.6
INO + BIRB 796	**900.5 (±85.5)**	778.4	909.3	973.5	941.0	**(489.1 (±23.7)**	454.5	503.2	493.0	505.5

NALM-6	3 hours treatment									
	untreated					VEN				
pretreatment (20 hours)	Mean (±SD)	n=1	n=2	n=3	n=4	Mean (±SD)	n=1	n=2	n=3	n=4
none	**606.2 (±103.3)**	621.1	523.7	746.5	533.6	**484.8 (±121.3)**	472.6	398.6	660.0	408.1
INO	**712.1 (±119.1)**	735.9	564.2	853.0	695.2	**276.6 (±52.5)**	243.1	236.7	351.0	275.5
BIRB 796	**647.7 (±102.1)**	711.1	521.6	747.5	610.4	**514.8 (±103.5)**	547.7	393.7	638.0	479.6
INO + BIRB 796	**547.2 (±71.4)**	554.7	446.8	614.0	573.4	**145.7 (±18.3)**	134.4	128.6	169.5	150.2

The assay to quantitate mitochondrial priming uses a defined VEN pulse to induce mitochondrial outer membrane permeabilization (MOMP). Mean fluorescence intensities (MFI) of TMRE stained cells are shown without (left: untreated) or after VEN treatment (right: VEN). Since the mitochondrial potential $\Delta\Psi_m$ (quantitated by MFI) varies under different conditions, VEN-mediated MOMP induction has to be referred to the actual $\Delta\Psi_m$ (MFI) for each sample and condition. The mean of TMRE-MFI change per condition is shown in Figure 4 A-D.

Supplementary Table 2: Cytogenetic aberrations of PDX samples.

PDX sample	cytogenetic aberration
L707	t(17;19)(q22;p13)
L4967	t(9;22)(q34;q11)
PDX1 KMT2A::AFF1	t(4;11)(q21;q23)
PDX2 KMT2A::MLLT1	t(11;19)(q23;p13)
PDX3 BCR::ABL1	t(9;22)(q34;q11)
PDX4 BCR::ABL1	t(9;22)(q34;q11)
PDX5 BCR::ABL1	t(9;22)(q34;q11)

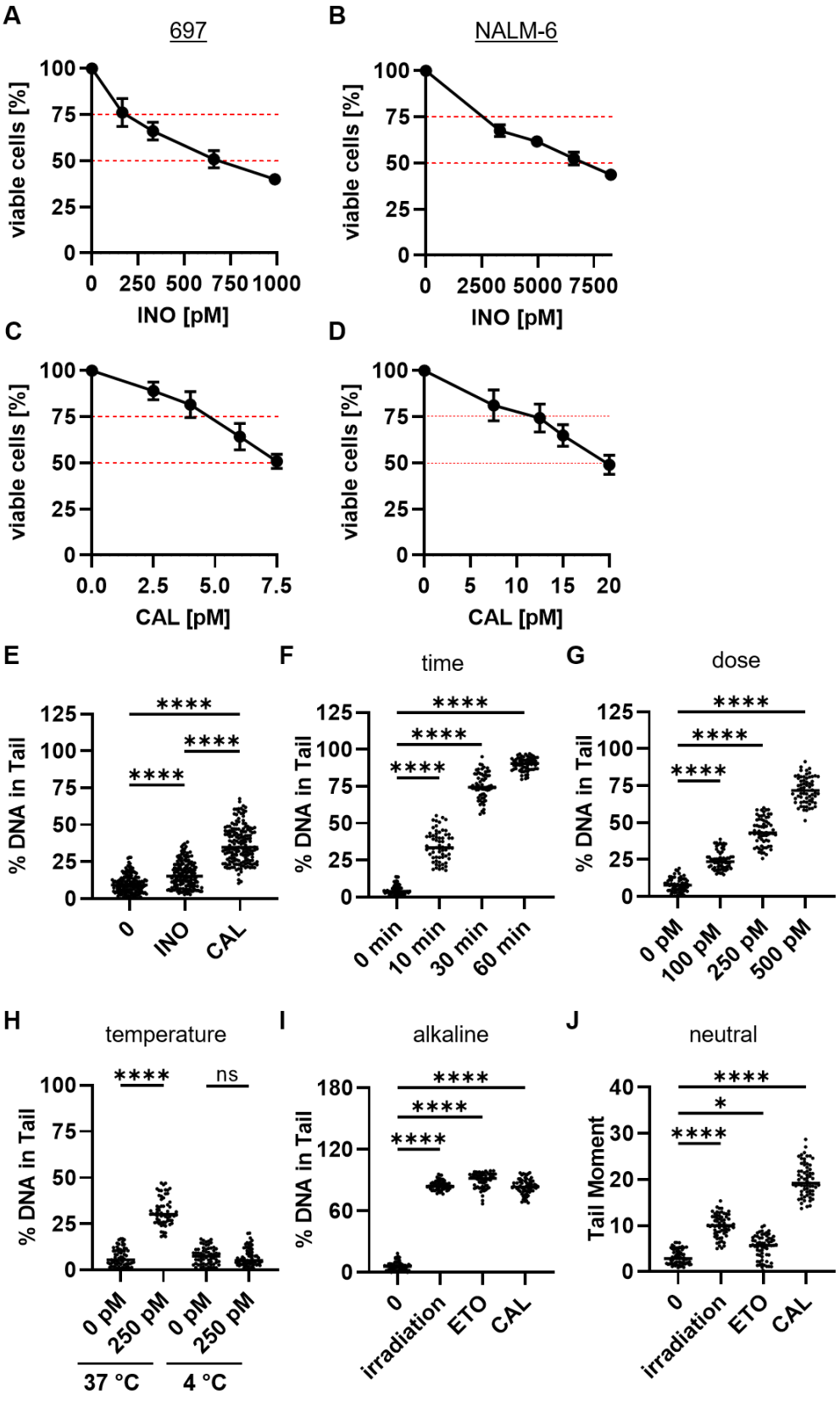

Figure S1: INO- and CAL-mediated cytotoxicity and DNA strand break induction. (A-D) 697 and NALM-6 cells were treated with increasing concentrations of INO (A+B) or CAL (C+D) for 24 h. IC75 and IC50 values were calculated for 697 (IC25 (INO): 180 pM, IC50 (INO): 660 pM, IC25 (CAL): 5 pM, IC50 (CAL): 7.5 pM) and NALM-6 cells (IC25

(INO): 2500 pM, IC50 (INO): 6600 pM, IC25 (CAL): 12.5 pM, IC50 (CAL): 20 pM). **(E)** NALM-6 cells were incubated with IC50 of INO (NALM-6: 6600 pM) for 6 h or with IC50 of CAL (NALM-6: 20 pM) for 2 h. **(F)** NALM-6 cells were treated with 500 pM CAL for 10 to 60 min **(G)** NALM-6 cells were treated with increasing CAL concentrations for 30 min or **(H)** with 250 pM CAL for 30 min at 37 °C and 4 °C. **(I+J)** Comparison of DNA strand breaks induced in NALM-6 cells by γ-irradiation (6 Gy), ETO (5 µM), and CAL (1 nM) after 30 min. Cells were analyzed in comet assays under alkaline (E-I) or neutral conditions (J). Each symbol represents one cell, with n=65 cells examined for each experimental condition. *p<0.05, ****p<0.0001, determined using the Kruskal-Wallis test and subsequent Dunn's multiple comparison test.

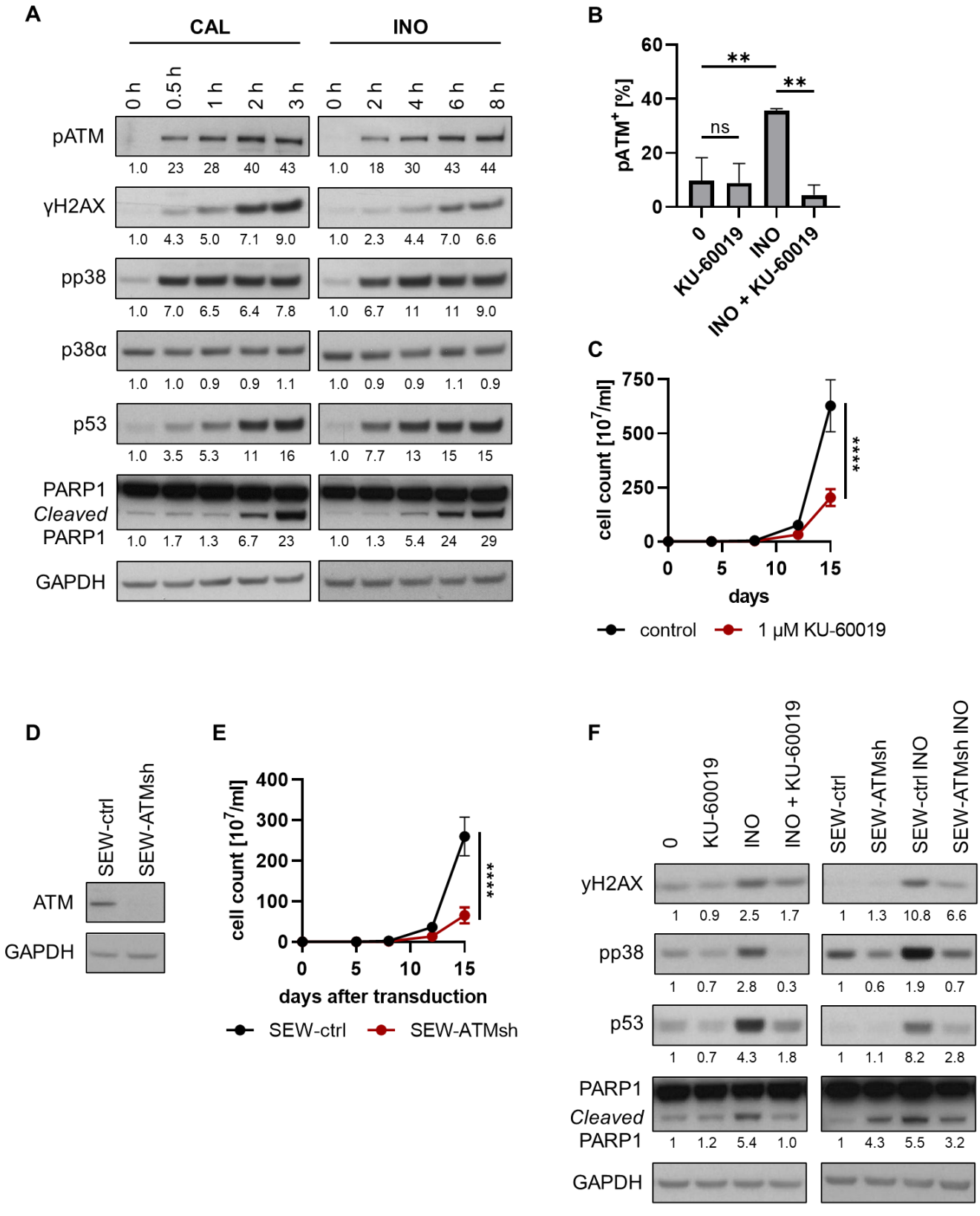

Figure S2: Reduction of DDR signaling by pharmacological inhibition or genetic depletion of ATM.. (A) NALM-6 cells were treated with their IC50 of CAL (20 pM) and INO (6.6 nM). The protein expression of pATM, γH2AX, pp38, p38α, p53, and cleaved PARP1 in

Western blot was quantified and normalized to GAPDH. **(B)** 697 cells were pretreated with 1 µM KU-60019 for 1 h. After the addition of 0.66 nM INO for 6 h, cells were fixed and stained with pATM antibody (n=3). **(C)** $2x10^5$ 697 cells were treated with 1 µM KU-60019 and counted on days 4, 8, 11, and 15 using trypan blue staining (n=3). **(D)** 697 cells were transduced with control (SEW-ctrl) or ATM-shRNA coding vector (SEW-ATMsh). At day 5 after transduction, cell lysates were prepared and protein expression of ATM was analyzed. **(E)** $2x10^5$ 697 cells were transduced and counted on days 4, 8, 11, and 15 using trypan blue staining (n=3). **(F)** 697 cells (pretreated with 1 µM KU-60019 for 1 h or transduced) were treated with 0.66 nM INO for 6 h. Protein expression of γH2AX, pp38, p53, and cleaved PARP1 in Western blot was quantified and normalized to GAPDH. **p<0.01, ****p<0.0001, p-values were calculated by one-way ANOVA (A) or two-way ANOVA (B+C) with the Bonferroni post hoc test.

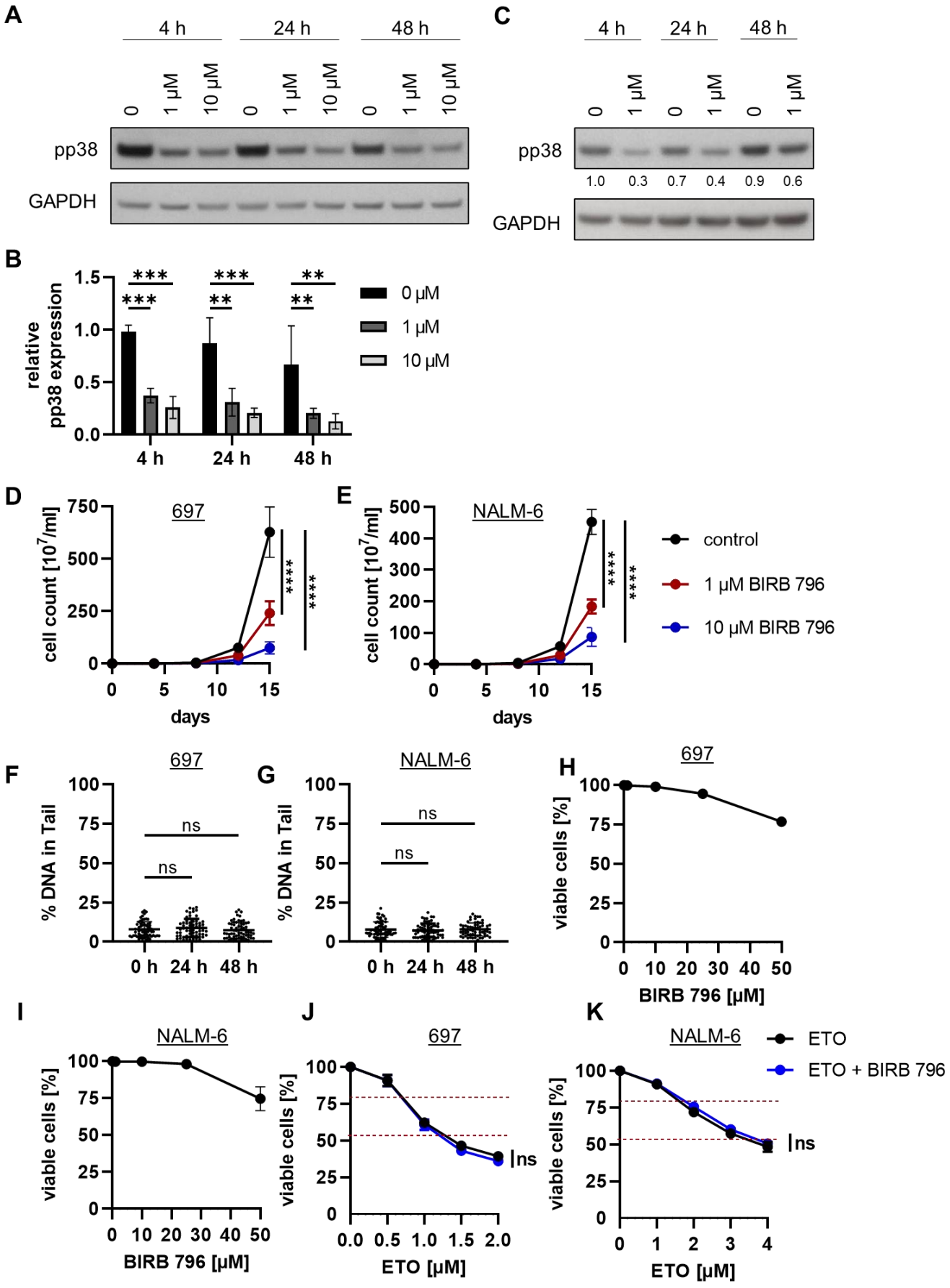
A
4 h
24 h
48 h
0
1 µM
10 µM
pp38
GAPDH
C
1.0
0.3
0.7
0.4
0.9
0.6
B
relative pp38 expression
0 µM
1 µM
10 µM
D
697
cell count [10^7/ml]
days
control
1 µM BIRB 796
10 µM BIRB 796
E
NALM-6
F
% DNA in Tail
ns
0 h
24 h
48 h
G
H
viable cells [%]
BIRB 796 [µM]
I
J
ETO [µM]
K
ETO
ETO + BIRB 796

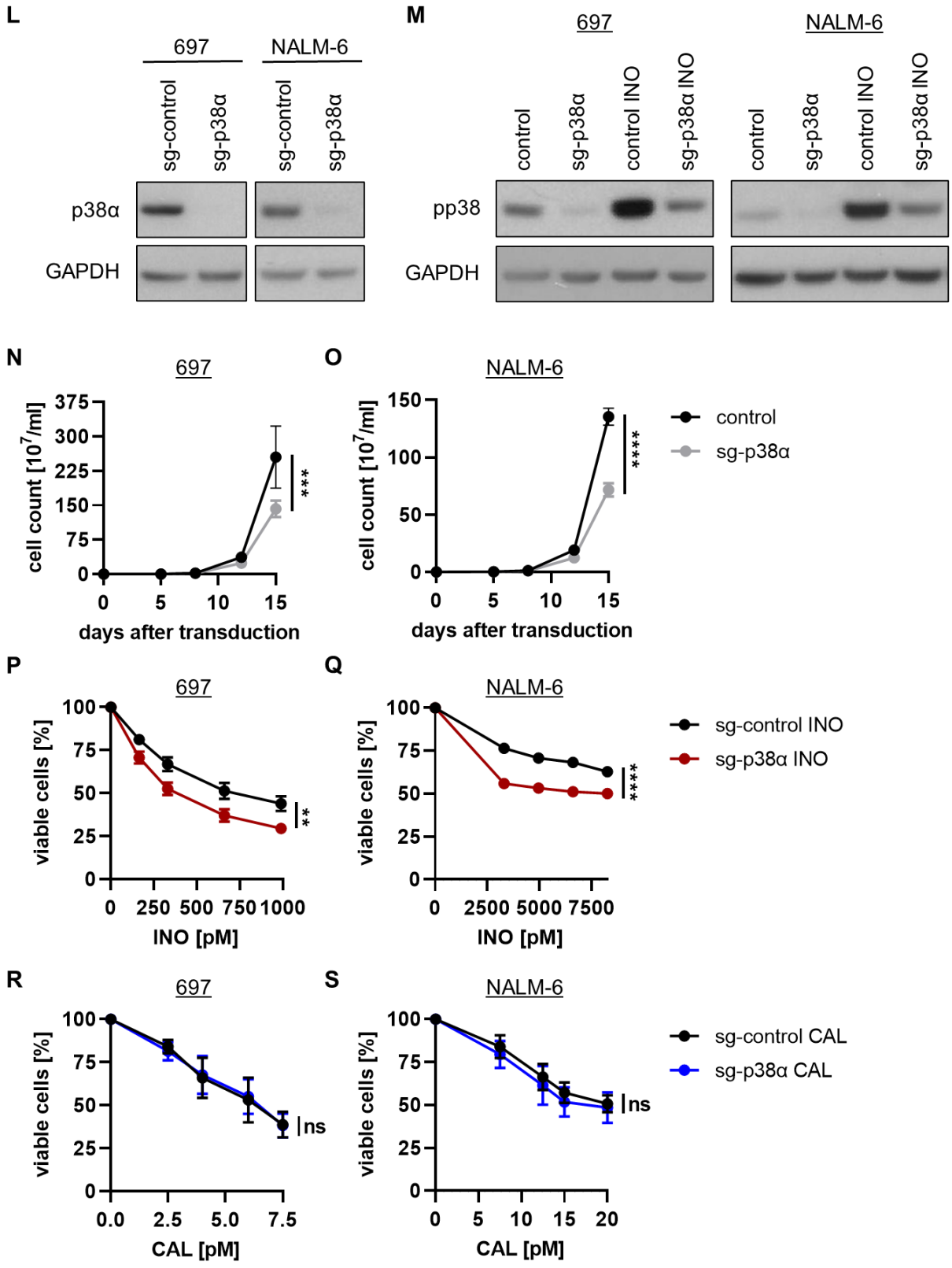

Figure S3: Impact of pharmacologic inhibition of p38 phosphorylation with BIRB 796 or genetic depletion of p38. (A+B) 697 cells were treated with 1 µM or 10 µM BIRB 796 for 4 h, 24 h, and 48 h. The expression of pp38 in Western blot was quantified and normalized to GAPDH (n=3). **(C)** NALM-6 cells were treated with 1 µM BIRB 796 for 4 h, 24 h, and 48 h and

the expression of pp38 and GAPDH was analyzed. **(D+E)** 697 and NALM-6 cells were treated with 1 µM or 10 µM BIRB 796 and counted on days 4, 8, 11, and 15 using trypan blue staining. **(F+G)** 697 and NALM-6 cells were treated with 1 µM BIRB 796 for 24 h and 48 h and analyzed in comet assays under alkaline conditions with n=65 cells examined for each experimental condition. **(H+I)** 697 and NALM-6 cells were treated with increasing concentrations of BIRB 796 for 48 h. Apoptotic cells were detected using PI staining and flow cytometric measurement (n=3). (J+K) 697 (J) and NALM-6 (K) cells were pretreated for 24 h with 1 µM BIRB 796, following treatment with increasing concentrations of Etoposide (ETO) for 24 h. Apoptotic cells were detected using PI staining (n=3). **(L-S)**697 and NALM-6 cells were transduced with control (sg-control) or p38α coding vector (sg-p38α). **(L)** At day 5 after transduction, cell lysates were prepared and protein expression of p38α was analyzed. **(M)** Transduced cells were treated with INO (697: 0.66 nM, NALM-6: 6.6 nM) for 6 h. Protein expression of pp38 and GAPDH was analyzed in Western blot. **(N+O)** $2x10^5$ 697 and NALM-6 cells were counted on days 4, 8, 11, and 15 after transduction using trypan blue staining (n=3). **(P-S)** Transduced 697 and NALM-6 cells were treated with increasing concentrations of INO (P+Q) or CAL (R+S) for 24 h. Apoptotic cells were detected using PI staining (n=3). **p<0.01, ***p<0.001, ****p<0.0001, p-values were calculated by two-way ANOVA with the Bonferroni post hoc test.

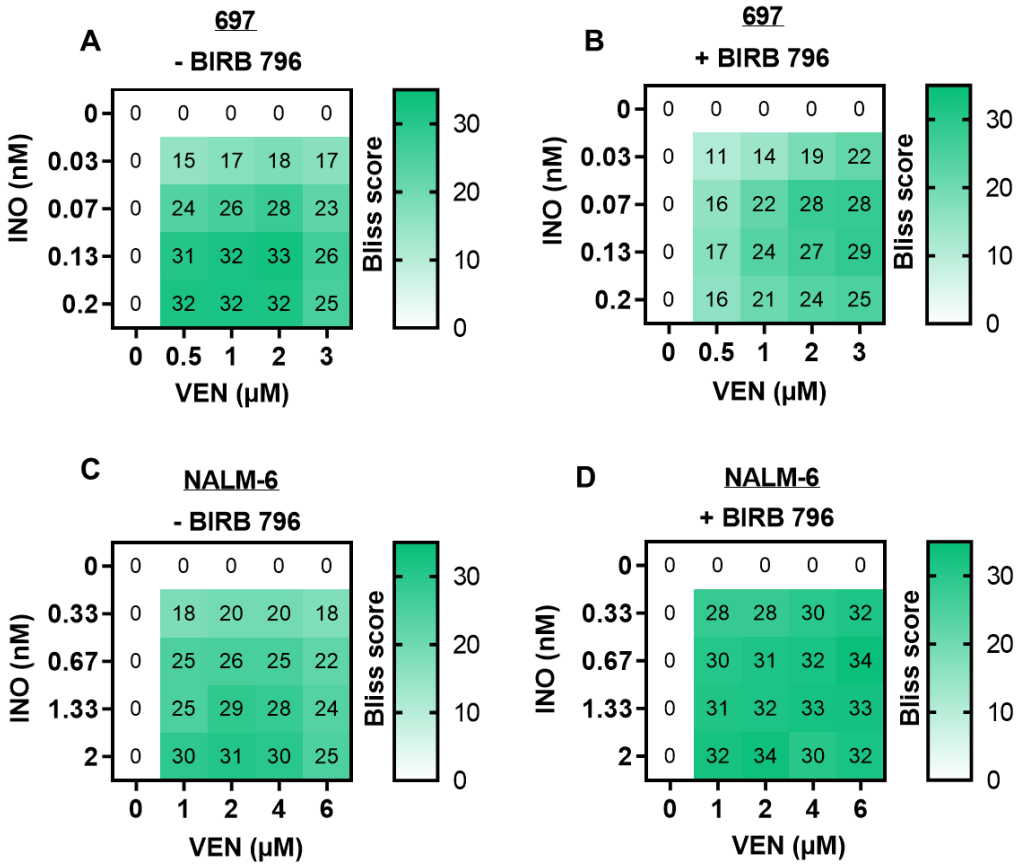

Figure S4: INO and VEN cytotoxicity acts synergistically in the presence of BIRB 796. 697 and NALM-6 cells were incubated in the absence or presence of 1 µM BIRB 796 with increasing concentrations of INO and VEN for 24 h followed by flow cytometric analysis of cell viability. Bliss Scores were calculated using SynergyFinder 3.0.

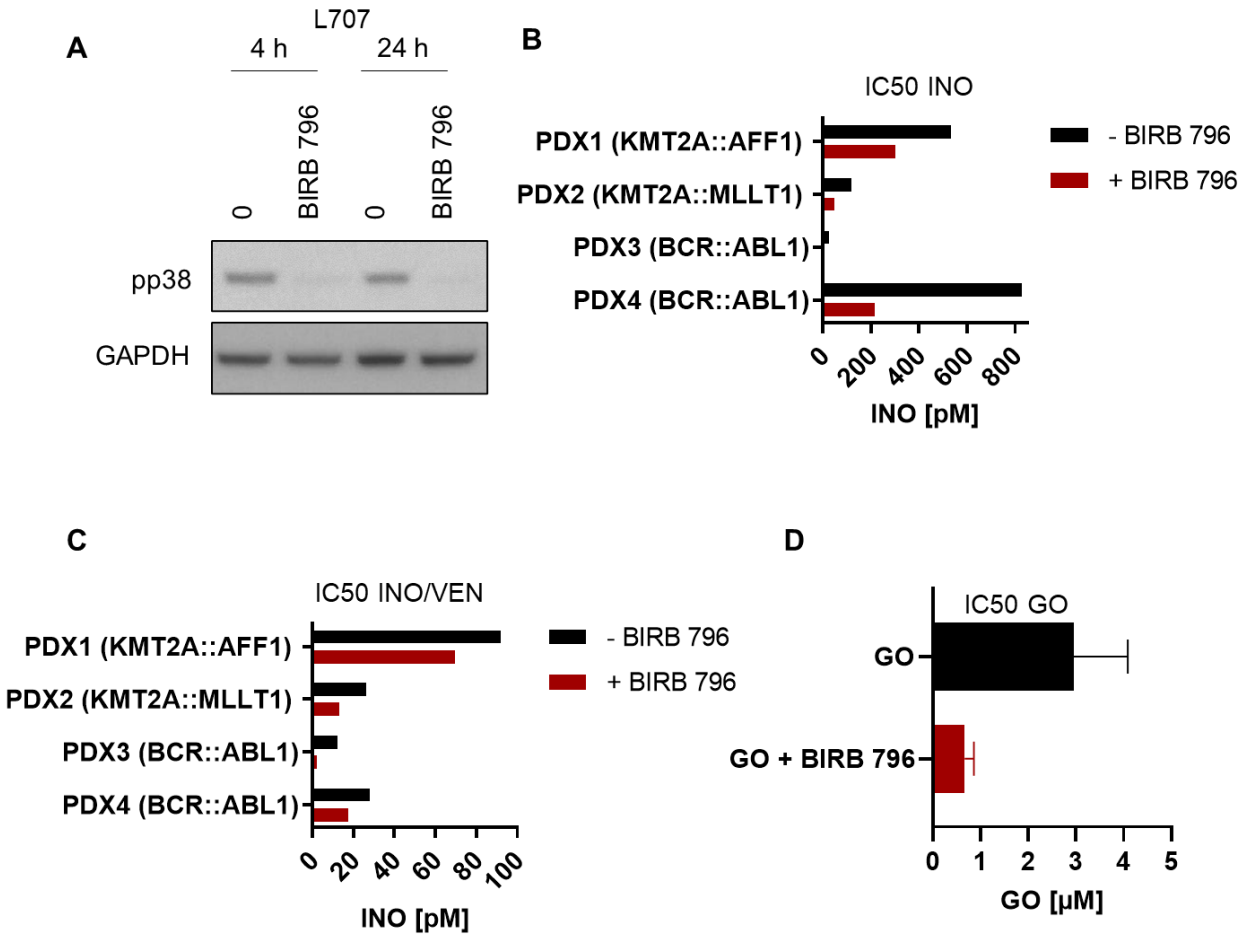

Figure S5: Pharmacologic p38 inhibition reduces IC50 of INO and the combination of INO and VEN in different PDX models in vitro. (A) L707 PDX cells were cultured on mesenchymal stem cells (MSCs) and treated with 10 µM BIRB 796 for 4 h and 24 h. Cell lysates were prepared, and expression of pp38 and GAPDH was analyzed in Western blot. **(B-C)** IC50 of (B) INO or (C) INO in the dual combination with VEN in the absence or presence of 10 µM BIRB 796. Cell viability was assessed by CD19/PI/CalceinAM staining and flow cytometry analysis. IC50s were calculated using CompuSyn Software. **(D)** IC50 of GO in PDX5 (BCR::ABL1) cells in the absence or presence of 10 µM BIRB 796. Cell viability was assessed by PI/CalceinAM staining and flow cytometric analysis. IC50s were calculated using CompuSyn Software.

A

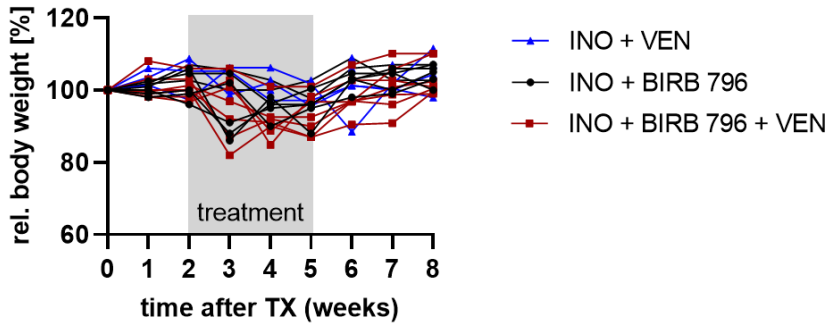

B

sample		viability BM (%)	huCD19+ BM (%)	viability spleen (%)	huCD19+ spleen (%)
control	n=6	81±14	99±1	86±3	93±4
INO + BIRB 796	n=4	73±25	89±13	88±4	86±8
INO + VEN	n=4	66±29	86±11	87±4	90±5
INO + VEN + BIRB 796	n=2	53±38	88±6	88±1	90±0.4

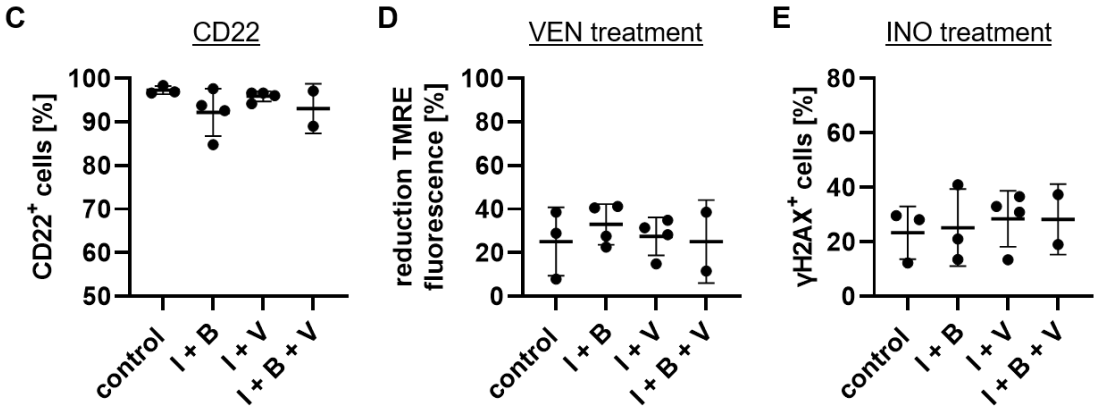

Figure S6: Body weight of L707 PDX transplanted NSG mice and analysis of r/r L707 PDX cells. (A) Body weight of L707 PDX mice treated with pharmacotherapy (INO + VEN, INO + BIRB 796, and INO + BIRB 796 + VEN). Grey bars indicate the oral treatment period of 3 weeks. Comparison of the lowest body weight per mouse revealed no significant differences between the treatment groups. **(B-E)** L707 PDX cells of relapsed mice were isolated from bone marrow and spleen upon reaching predefined endpoint criteria. **(B)** Viability of L707 PDX cells isolated from bone marrow (BM) and spleen. Cells were stained with a human anti-CD19 antibody, and the proportion of human CD19-positive cells among total BM or spleen cells from the mice is shown. **(C)** Surface expression of human CD22 in the human CD45-positive cell population of r/r L707 cells. **(D)** MOMP induction in r/r L707 PDX cells. Cells from the spleen were treated for 3 h with 1 µM VEN. Viable cells were gated based on the FSC/SSC profile. The MFI of untreated cells was set as 100%. **(E)** Flow cytometry analysis of γH2AX expression

of r/r L707 PDX cells from the spleen. Cells were treated for 6 h with 6.6 nM InO. P-values were calculated by one-way ANOVA with Bonferroni post hoc test. No significant differences were observed.

Supplementary References

1. Findley HW, Jr., Cooper MD, Kim TH, Alvarado C, Ragab AH. Two new acute lymphoblastic leukemia cell lines with early B-cell phenotypes. Blood. 1982;60(6):1305-9.
2. Hurwitz R, Hozier J, LeBien T, et al. Characterization of a leukemic cell line of the pre-B phenotype. Int J Cancer. 1979;23(2):174-80.
3. Scherr M, Battmer K, Ganser A, Eder M. Modulation of Gene Expression by Lentiviral Mediated Delivery of Small Interfering RNA. Cell Cycle. 2003;2(3):251-7.
4. Brummelkamp TR, Bernards R, Agami R. A System for Stable Expression of Short Interfering RNAs in Mammalian Cells. Science. 2002;296(5567):550-3.
5. Ran FA, Hsu PD, Wright J, et al. Genome engineering using the CRISPR-Cas9 system. Nat Protoc. 2013;8(11):2281-308.
6. Sieve I, Ricke-Hoch M, Kasten M, et al. A positive feedback loop between IL-1beta, LPS and NEU1 may promote atherosclerosis by enhancing a pro-inflammatory state in monocytes and macrophages. Vascul Pharmacol. 2018;103-105:16-28.
7. Venturini L, Battmer K, Castoldi M, et al. Expression of the miR-17-92 polycistron in chronic myeloid leukemia (CML) CD34+ cells. Blood. 2007;109(10):4399-405.
8. Chou TC. Drug combination studies and their synergy quantification using the Chou-Talalay method. Cancer Res. 2010;70(2):440-6.
9. Ianevski A, Giri AK, Aittokallio T. SynergyFinder 3.0: an interactive analysis and consensus interpretation of multi-drug synergies across multiple samples. Nucleic Acids Res. 2022;50(W1):W739-W43.
10. Kirchhoff H, Karsli U, Schoenherr C, et al. Venetoclax and dexamethasone synergize with inotuzumab-ozogamicin induced DNA damage signaling in B-lineage ALL. Blood. 2021;137(19):2657–61.